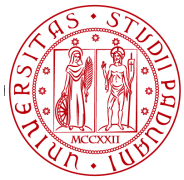

UNIVERSITÀ
DEGLI STUDI
DI PADOVA

Sede Amministrativa: Università degli Studi di Padova

Dipartimento di Scienze Biomediche

SCUOLA DI DOTTORATO DI RICERCA IN: BIOSCIENZE E BIOTECNOLOGIE

INDIRIZZO: NEUROBIOLOGIA

CICLO: XXIV

FUNCTIONAL CONSEQUENCES OF FAMILIAL HEMIPLEGIC MIGRAINE TYPE 1 MUTATIONS ON CORTICAL ACTIVITY

Direttore della Scuola: Ch.mo Prof. Giuseppe Zanotti

Coordinatore d'indirizzo: Ch.mo Prof. Daniela Pietrobon

Supervisore: Ch.mo Prof. Daniela Pietrobon

Dottorando: Michele Sessolo

INDEX

	SUMMARY	1
	RIASSUNTO	5
1.	**INTRODUCTION**	9
1.1	Migraine	9
1.2	Neurobiology of migraine	9
1.3	Familial Hemiplegic Migraine	13
1.4	Voltage-gated calcium channels	14
1.4.1	Structure of voltage-gated Ca^{2+} channels	15
1.4.2	Ca^{2+} channels localization and function	18
1.4.3	Presynaptic Ca^{2+} channels controlling neurotransmission	19
1.5	Synaptic plasticity	20
1.6	Functional consequences of FHM1 mutations	23
1.7	Organization of the cortex	27
1.8	Cellular populations in the cortex	27
1.9	Spontaneous cortical activity	30
2.	AIMS OF WORK	33
3.	**RESULTS**	35
3.1	Characterization of excitatory and inhibitory connection between pyramidal cells and somatostatin interneurons in GIN mice	35
3.1.1	Characterization of excitatory connection between PYR cells and GIN interneurons	35
3.1.2	Involvement of calcium channels in the control of glutamate neurotransmitter release at the excitatory synapses between PYR cells and GIN interneurons	37
3.1.3	Characterization of inhibitory connection between GIN interneurons and PYR cells	40
3.1.4	Involvement of calcium channels in the control of glutamate neurotransmitter release at the inhibitory synapses between GIN interneurons and PYR cells	41
3.1.5	Characterization of firing properties of GIN interneurons	43

3.2.1 Spontaneous excitatory and inhibitory activity recorded from layer 2/3 PYR cell of primary somatosensory cortex in WT mice 46
3.2.2 Large bursts occur synchronously in nearby PYR cells and generate up states in current clamp 48
3.2.3 Excitatory and inhibitory uncorrelated asynchronous sPSCs in PYR cells of WT and R192Q FHM1 KI mice 50
3.2.4 Spontaneous synchronous bursts of sPSCs in layer 2/3 PYR cells of WT and R192Q FHM1 KI mice 52
4 DISCUSSION 57
4.1 Study of excitatory and inhibitory synaptic transmission between pyramidal cell and fluorescent somatostatin-expressing interneurons 57
4.2 Study of the total amount of excitatory and inhibitory synaptic charge onto a pyramidal cell 59
5 **MATERIALS AND METHODS** 63
5.1 Experimental procedures for the study of spontaneous activity 63
5.1.1 Animals 63
5.1.2 Coronal slices solutions 63
5.1.3 Slice preparation 63
5.1.4 Microscope 64
5.1.5 Patch clamp technique 64
5.1.6 Patch clamp set up and recordings 65
5.1.7 Data analysis 67
5.2 Experimental procedures for the study of connection between pyramidal cells and fluorescent SOM+ interneurons. 67
5.2.1 Animals 67
5.2.2 Thalamocortical slices preparation 68
5.2.3 Patch clamp set up and recordings 68
5.2.4 Data analysis 70
5.3 Morphological reconstruction of neurons 71
Reference list 73
Abbreviations 79

SUMMARY

Missense mutations in the gene that encodes the pore-forming α_1 subunit of voltage-gated CaV2.1 (P/Q-type) Ca^{2+} channels cause a rare autosomal dominant subtype of migraine with aura: Familial Hemiplegic Migraine type 1 (FHM1). Knock-in (KI) mice carrying FHM1 mutations show increased P/Q-type Ca^{2+} current density in central neurons including cortical pyramidal (PYR) cells (Tottene et al., 2009; van den Maagdenberg et al., 2004). The investigation of neurotransmission in neuronal microcultures and in acute cortical slices of R192Q FHM1 knock-in (KI) mice revealed increased strength of excitatory synaptic transmission due to increased action potential-evoked Ca^{2+} influx through presynaptic P/Q-type Ca^{2+} channels and increased probability of glutamate release at cortical PYR cell synapses of mutant mice; in striking contrast, inhibitory neurotransmission at connected pairs of fast-spiking interneurons and PYR cells was unaltered in FHM1 KI mice, despite being initiated by P/Q-type Ca^{2+} channels (Tottene et al., 2009). The finding of different effects of FHM1 mutation at different synapses suggests that episodic disruption of the excitation-inhibition balance may underlie the increased susceptibility to cortical spreading depression (CSD), the phenomenon underlying migraine aura and a likely trigger of the migraine headache mechanisms. To further test this hypothesis I focused on the effect of FHM1 mutations at other cortical synapses. To study the synaptic connections involving somatostatin-positive (SOM^+) interneurons we took advantage of GIN (GFP-expressing Inhibitory Neurons) mice which express an enhanced GFP restricted to a subpopulation somatostatin-positive (SOM^+) interneurons (GIN interneurons)(Oliva et al., 2000).

I performed double patch-clamp experiments on acute slices of somatosensory cortex to study excitatory and inhibitory synaptic transmission between layer 2/3 PYR cells and GIN interneurons in GIN mice. I have found that the excitatory synapse onto SOM^+ interneurons shows short-term facilitation during trains of action potentials at 25 Hz suggesting that these interneurons can be recruited during sustained activity; in contrast, the inhibitory synapse between GIN interneurons and PYR cells displayed a relatively weak short-term depression during trains of action potentials at 20 Hz.

Since voltage-gated Ca^{2+} channels controlling neurotransmitter release at these synapses are not known I performed pharmacological experiments in the presence of the specific inhibitors of P/Q- (ω-Agatoxin IVA) and N-type (ω-Conotoxin GVIA) Ca^{2+} channels to determine the contribution of these Ca^{2+} channels in controlling neurotransmitter

release. I found that both P/Q- and N-type Ca^{2+} channels contribute to control GABA release at the GIN interneuron synapses and glutamate release at the PYR cell synapses, with a predominant role of the P/Q-type Ca^{2+} channels. Given the important role of P/Q-type Ca^{2+} channels in controlling neurotransmitter release at these synapses it will be interesting to study excitatory and inhibitory neurotransmission between PYR cells and GIN interneurons in GIN mice carrying the R192Q FHM1 mutation.

To test the general hypothesis that FHM1 mutations might lead to an unbalance between inhibition and excitation towards excitation, I collaborated with Alessandra Fabbro in studying the total excitatory and inhibitory synaptic charge received by a layer 2/3 PYR cell during ongoing network activity without any type of stimulation. We performed voltage clamp recordings at the reversal potential for the inhibitory inputs (-79 mV) and at reversal potential for the excitatory inputs (+10 mV) to isolate spontaneous excitatory post-synaptic currents (sEPSC) and spontaneous inhibitory post-synaptic currents (sIPSCs) respectively.

Voltage-clamp recordings of sEPSCs and sIPSCs revealed two types of activity. The first is the spontaneous postsynaptic currents (sPSCs) which arise from uncorrelated and random spontaneous activity of presynaptic excitatory and inhibitory neurons which make synapses onto the patched cell; the second is characterized by high amplitude bursts of sPSCs which arise from correlated activity of a large population of presynaptic connected neurons generated through network mechanisms.

Integrals of the uncorrelated sPSCs in slices of WT and R192Q KI mice show that the excitatory synaptic charge of uncorrelated sEPSCs is larger in R192Q KI mice compared to WT mice, which is consistent with the enhanced glutamate release, and increased excitatory synaptic transmission found at PYR cells synapses of KI mice (Tottene et al, 2009). The inhibitory synaptic charge of uncorrelated sPSCs is not altered in KI mice which in accordance with unaltered inhibitory transmission at synapses of FS and other types of intemeurons contributing to the sIPSCs (Tottene et al, 2009).

The analysis of the large bursts of correlated sPSCs showed that both excitatory and inhibitory burst charge are increased in R192Q KI mice but the ratio of excitatory to inhibitory burst charges is similar in WT and KI mice. These findings indicate that during the spontaneous network activity the excitation-inhibition balance is not altered in R192Q KI mice. The increase of both excitatory and inhibitory burst charges in KI mice is caused by an increase of burst frequency. As a consequence, the fraction of time

spent by the cortical network in the spontaneous synchronous activity is larger in KI than WT mice.

RIASSUNTO

L'emicrania emiplegica familiare di tipo 1 (FHM1), un raro sottotipo di emicrania con aura, è causata da mutazioni missenso nel gene che codifica per la subunità α_1 dei canali del calcio (Ca^{2+}) voltaggio dipendenti $Ca_V2.1$ (tipo P/Q).
I topi omozigoti knock-in (KI) recanti la mutazione FHM1 R192Q presentano, in granuli di cervelletto e in cellule piramidali corticali, un aumento della densità di corrente Ca^{2+} di tipo P/Q (Tottene et al., 2009; van den Maagdenberg et al., 2004). Lo studio della trasmissione sinaptica in microcolture neuronali e in fettine acute di cervello di topi KI ha dimostrato: un aumento della forza della trasmissione sinaptica eccitatoria dovuto ad un aumento dell'influsso di Ca^{2+} attraverso i canali di tipo P/Q localizzati a livello presinaptico e un aumento della probabilità di rilascio di glutammato alle sinapsi corticali di cellule piramidali (PYR) dei topi mutanti. Al contrario, la trasmissione sinaptica inibitoria studiata tra interneuroni *fast-spiking* (FS) e cellule PYR è risultata essere inalterata nei topi KI nonostante i canali di tipo P/Q siano coinvolti nel rilascio anche a queste sinapsi inibitorie (Tottene et al., 2009). Queste evidenze suggeriscono che alterazioni episodiche del bilancio tra eccitazione ed inibizione in corteccia possano essere alla base dell'aumentata suscettibilità alla *cortical spreading depression* (CSD, il fenomeno che sottende l'aura emicranica). Per confermare questa ipotesi mi sono concentrato sugli effetti delle mutazioni FHM1 ad altre sinapsi corticali. La connessione sinaptica tra cellule PYR ed interneuroni positivi alla somatostatina (SOM^+) corrispondenti alle cellule di Martinotti in ratto, è stata studiata in topo sfruttando la disponibilità di un ceppo transgenico (*GFP-expressing interneurons*, GIN) che esprimono la GFP (*green fluorescent protein*) in una sottopopolazione di interneuroni positivi alla somatostatina per lo più considerati cellule di Martinotti (Oliva et al., 2000; Fanselow et al., 2008).
Ho eseguito esperimenti di doppio patch-clamp su fettine acute di cervello di corteccia somatosensoriale primaria per studiare la connessione eccitatoria tra cellule PYR e interneuroni SOM (da qui in poi chiamati interneuroni GIN) e la connessione inibitoria reciproca in topi GIN. Ho trovato che la connessione eccitatoria PYR-GIN presenta facilitazione a breve termine (*short term facilitation*) in risposta a treni di potenziali d'azione (*action potentials, APs*) a 25 Hz suggerendo che questi interneuroni possono essere reclutati da cellule PYR durante periodi di attività neuronale sostenuta; al contrario la sinapsi inibitoria GIN-PYR è caratterizzata da una debole depressione a breve termine (*short term depression*, STD) in risposta a treni di APs a 20 Hz.

I canali del Ca^{2+} che controllano il rilascio di neurotrasmettitore ad entrambe le sinapsi eccitatorie ed inibitorie tra cellule PYR ed inteneuroni GIN non sono noti; pertanto ho utilizzato un approccio farmacologico perfondendo nella soluzione extracellulare inibitori di specifici canali del Ca^{2+}, ω-Agatoxin IVA per inibire i canali di tipo P/Q e ω-Conotoxin GVIA per inibire i canali di tipo N, per determinare il loro coinvolgimento nel controllo del rilascio di neurotrasmettitore. Questi esperimenti hanno evidenziato che i canali di tipo P/Q con un ruolo predominante e i canali di tipo N sono coinvolti e cooperano nel rilascio di neurotrasmettitore sia alla sinapsi eccitatoria PYR-GIN che a quella inibitoria GIN-PYR. Dato il coinvolgimento dei canali di tipo P/Q sarà interessante studiare eventuali alterazioni della trasmissione sinaptica eccitatoria ed inibitoria tra cellule PYR ed inteneuroni GIN in topi KI per la mutazione R192Q incrociati con i topi GIN.

Per verificare l'ipotesi generale che le mutazioni FHM1 possano portare ad uno sbilanciamento in corteccia tra inibizione ed eccitazione (a scapito di quest'ultima), ho collaborato con la Dott.ssa Alessandra Fabbro nello studio della carica sinaptica eccitatoria ed inibitoria totale che una cellula PYR dello strato 2/3 riceve durante l'attività di *network* in assenza di stimolazione. Abbiamo effettuato registrazioni di *voltage clamp* al potenziale di reversione degli input inibitori (-79 mV) e a quello degli input eccitatori (+ 10 mV) per poter isolare rispettivamente le correnti postsinaptiche eccitatorie (*spontaneous excitatory postsynaptic currents*, sEPSCs) e quelle inibitorie (*spontaneous inhibitory postsynaptic currents*, sIPSCs).

Gli esperimenti di *voltage clamp* hanno messo in evidenza due tipi di attività. La prima è caratterizzata da correnti postsinaptiche spontanee (*spontaneous postsynaptic currents*, sPSCs) generate da input non correlati, eccitatori o inibitori, che arrivano in modo casuale da cellule eccitatorie PYR ed interneuroni inibitori connessi con la cellula da cui si esegue la registrazione; il secondo tipo di attività è caratterizzato da *burst* di PSCs di grandi ampiezze e che originano dall'attività correlata, forse attraverso meccanismi di *network*, di grandi popolazioni di cellule eccitatorie o inibitorie che formano sinapsi sulla cellula registrata.

Il calcolo dell'integrale delle sPSCs non correlate in fette acute di corteccia somatosensoriale da topi WT e KI indicano che la carica eccitatoria delle sPESCs non correlate è aumentata nei topi KI in accordo con l'aumentato rilascio di glutammato e un aumentata trasmissione sinaptica eccitatoria alle sinapsi tra cellule PYR di topi KI (Tottene et al., 2009); al contrario la carica inibitoria mediata dalle sIPSCs non correlate

risulta non essere alterata nei topi KI in accordo con l'inalterata trasmissione sinaptica inibitoria tra interneuroni FS e cellule PYR (Tottene et al., 2009).

L'analisi delle aree dei grandi *burst* di input correlati ha evidenziato che sia la carica eccitatoria che quella inibitoria dei *burst* sono aumentate nei topi KI ma il rapporto tra carica eccitatoria ed inibitoria risulta essere inalterata nei topi KI. Questi risultati indicano che durante l'attività spontanea di network il bilancio tra eccitazione ed inibizione non è alterato.

L'incremento della carica eccitatoria ed inibitoria nei topi KI è dovuto ad un aumento nella frequenza dei *burst* da cui consegue un aumento nel tempo trascorso dalla corteccia nell'attività spontanea correlata nei topi KI.

1. INTRODUCTION

1.1 Migraine

Migraine is a common, highly disabling episodic disorder that affects more than 10% of the population in western countries with a higher prevalence in women (15-25%) than men (6-8%). Given its strong impact in the quality of life for individuals and society, migraine is classified by the World Health Organization as one of the 20 most disabling disorders (Pietrobon and Striessnig, 2003).

Migraine can be divided in two major subtypes: migraine with aura (MA) and without aura (MO).

Migraine attacks are typically characterized by unilateral pulsating severe headache lasting from 4 to 72 hours often associated with nausea phono- and photophobia (MO). At least one third of patients are affected by aura which precedes the headache (MA). Aura symptoms can last up to 60 minutes and are usually characterized by visual scotoma with scintillanting border drifting slowly across the visual field. Aura can also affect other senses or cause speech deficits (Pietrobon and Striessnig, 2003).

Even though migraine has a strong (up to 50%) genetic component (higher in MA than MO), characterized by a multifactorial polygenic inheritance, external and internal factors (migraine triggers) can modulate migraine threshold (Pietrobon 2005a).

Several loci have been linked to migraine (both MA and MO) but the causative genes have not been identified yet. One exception is represented by Familial Hemiplegic Migraine (FHM), a rare autosomal subtype of MA characterized by dominant inheritance: (Pietrobon 2005a; (Pietrobon and Striessnig, 2003).

1.2 Neurobiology of migraine

The development of migraine headache depends on the activation of the trigeminovascular system (Pietrobon and Striessnig, 2003). Indeed, pain sensitivity within the skull is restricted primarily to the meningeal blood vessels, which are densely innervated by nociceptive sensory afferent fibers of the ophthalmic division of the trigeminal nerve (Pietrobon, 2005a; Pietrobon and Striessnig, 2003). In different animal models, including non human primates, activation of the meningeal trigeminovascular afferents leads to activation of second order dorsal horn neurons in the trigeminal

nucleus caudalis (TNC) and of the upper two divisions of the cervical spinal cord (Figure 1.1, arrows 1, 3). Impulses are then carried rostrally to brain structures involved in the perception of pain, including several thalamic nuclei and the ventrolateral area of the caudal periaqueductal gray region (PAG) (Figure 1.1, arrows 4, 5). The PAG is involved in the craniovascular pain through both ascending projections to the thalamus and descending modulation (mainly inhibitory) of nociceptive afferent information via projections to serotonergic neurons in the magnus raphae nucleus (MRN). Activation of the trigeminovascular afferents also triggers release of vasoactive neuropeptides contained in the peripheral nerve endings, including neurokinin A (NKA), calcitonin gene-related peptide (CGRP), substance P (SP) (Figure 1.1, inset). The activation of parasympathetic pathway through the trigeminal ascending projections involves the superior salivatory nucleus (SSN) and superior sphenopalatine ganglion (SPG) which in turn leads the release of others vasoactive neuropeptides as Ach, nitrix oxide (NO), vasoactive intestinal peptide (VIP) in the meninges (Figure 1.1, arrows 6 and 7 and inset). In animal studies neuropeptides released by trigeminal ganglion stimulation produces vasodilatation of the meningeal vessels (mainly due to CGRP), plasma extravasation and mast cell degranulation with secretion of other proinflammatory substances in the *dura* (neurogenic inflammation).

Evidence that activation of the trigeminovascular system occurs in humans during migraine is provided by the increased level of CGRP found in both the external and internal jugular blood during migraine attacks. Moreover CGRP return to normal levels after sumatriptan (an anti-migraine drug) treatment and this is accompanied by headache relief (Pietrobon, 2005a; Pietrobon and Striessnig, 2003).

The mechanism leading to activation of the trigeminovascular system, and the following migraine headache, is still debated but recent findings show the untenableness of the vascular theory in which the symptoms of migraine aura are caused by transient ischemia induced by vasoconstriction, and the headache arises from rebound abnormal vasodilatation of intracranial arteries and consequent mechanical activation of perivascular sensory fibers (Pietrobon 2005a).

It is now generally accepted that the primary cause of migraine headache lies in the brain. Nevertheless the mechanisms that lead to trigeminovascular system activation remain largely understood. Recent findings point to cortical spreading depression (CSD) as a key player in the pathogenesis of migraine (Pietrobon, 2005a; Pietrobon and Striessnig, 2003).

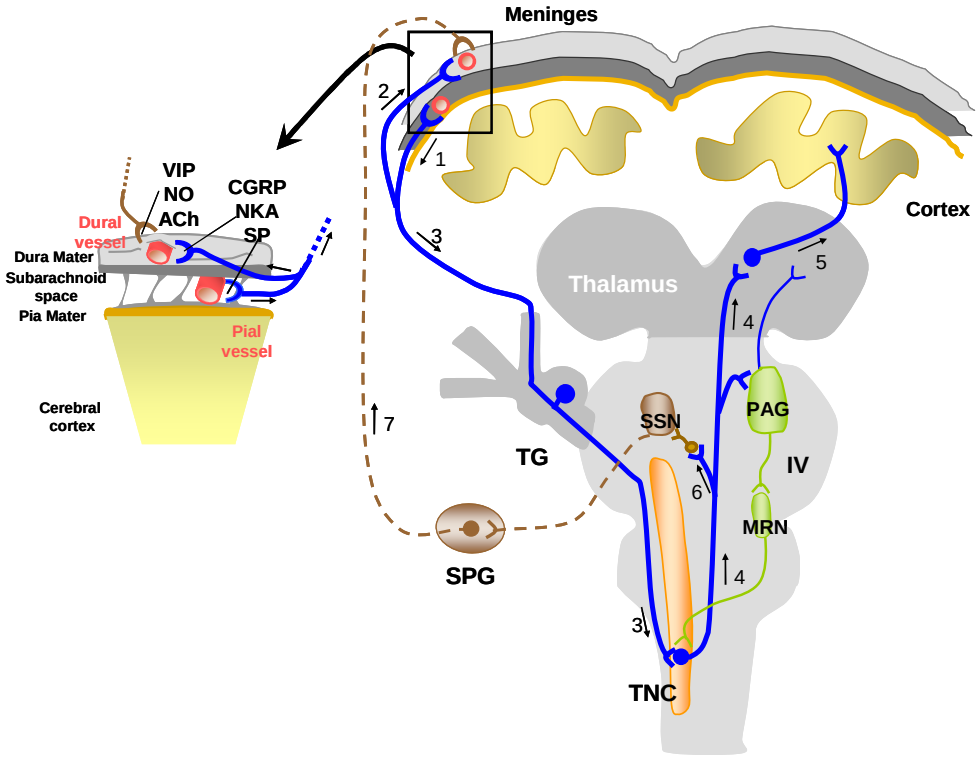

Figure 1.1. Neuronal structures and pathways involved in the trigeminovascular activation and modulation of cephalic pain (from Pietrobon 2005a).

IV, fourth ventricle; ACh, acetylcholine; CGRP, calcitonin gene-related peptide; PAG, periaqueductal grey region; MRN, magnus raphe nucleus; NKA, neurokinin A; NO, nitrix oxide; SP, substance P; SPG, superior sphenopalatine ganglion; SSN, superior salivatory nucleus; TG, trigeminal ganglion; TNC, trigeminal nucleus pars caudalis; VIP, vasoactive intestinal peptide.

CSD is a slowly propagating wave (2-6 mm/min) characterized by strong neuronal and glial depolarization that can be elicited in animals by focal mechanical (pinprick), electrical or chemical (high concentrations of K^+) stimulation, by inhibition of the Na^+/K^+ ATPase and by other stimuli of the cerebral cortex (Moskowitz, 2007; Pietrobon, 2007). This depolarization generates a transient neuronal intense spike activity, followed by long-lasting neuronal suppression (Pietrobon, 2005a; Pietrobon and Striessnig, 2003). The CSD was first described by Leão in the rabbit cortex in 1944 (Leão, 1944). The depolarization phase is associated with an initial transient vasodilatation followed by an increase in regional cerebral blood flow (rCBF). The phase of reduced neuronal activity is by contrast associated with a reduction in rCBF subsequent to a sustained vasoconstriction (Lauritzien 2001).

Neuroimaging studies indicate that CSD is responsible for migraine aura (Pietrobon and Striessnig, 2003). High-field functional magnetic resonance imaging (fMRI) studies

were used to follow blood oxygenation level dependent (BOLD) signals in three patients while experiencing visual aura. These studies demonstrated a correlation between the initial features of the aura percept (scintillations beginning in the paracentral left visual field) and the initial increase in the mean BOLD signal which reflects cortical hyperaemia. The mean BOLD level subsequently decreases in correlation with the scotoma following the scintillations. The BOLD signal changes developed first in the extrastriate cortex, contralateral to the visual changes, and then slowly migrated (3.5 mm/min) towards more anterior regions of the visual cortex, representing peripheral visual fields. This is in agreement with the progressive movement of the scintillations and scotoma from the center of vision towards the periphery (Hadjikhani et al., 2001). Magnetoencephalography (MEG) studies provided additional evidences that CSD underlies migraine aura in human visual cortex (Pietrobon 2005a).

Spreading cerebral perfusion changes have also been observed in migraine without aura, raising the possibility that CSD within clinically silent areas of the cerebral cortex may play a role in the pathophysiology of migraine without aura (Moskowitz, 2007; Pietrobon, 2005a)

Studies in animal models support the idea that CSD might be crucial for the induction of migraine headache. It has been shown that CSD can activate meningeal trigeminal afferents and long-lasting blood-flow enhancement within the middle meningeal artery and plasma protein leakage in the *dura mater* (Zhang et al., 2010; Bolay et al., 2002).

The precise mechanism linking CSD to activation of the meningeal nociceptors is however not completely understood. CSD induces a large increase in the concentration of K+ and H+ ions, NO, ATP, arachidonic acid, and prostaglandins in the cortex extracellular fluid. Many of these substances, can activate the meningeal trigeminovascular afferents, either directly or by causing perivascular inflammation (Pietrobon, 2005b). Moreover it has been shown that CSD causes changes in gene expression that lasts from hours to days raising therefore the possibility that CSD can regulate long-term changes in the sensitivity of trigeminovascular nociceptive pathways (Pietrobon, 2005b).

Nevertheless, a direct link between CSD and headache in patients has not been proved. The mechanisms that make the brain of migraineurs susceptible to episodic “spontaneous” CSDs in response to specific triggers such as stress or intense, repetitive long lasting sensory stimulation remain unknown. Migraineurs are hypersensitive to any kind of sensory overload and there is strong evidence of altered cortical excitability and

abnormal processing of sensory information in their brain during the period between migraine attacks (Pietrobon, 2005a; Pietrobon and Striessnig, 2003). The mechanisms underlying the interictal abnormalities in cortical activity are controversial and their relationship to susceptibility and/or occurrence of CSD is unclear.

1.3 Familial Hemiplegic Migraine

Familial Hemiplegic Migraine (FHM) is a rare autosomal dominant subtype of MA. The main symptoms of the headache and aura of FHM are similar to those of MA but the aura is additionally characterized by obligatory motor symptoms (weakness or paralysis often unilateral) and they last longer than in MA. In addition to typical FHM attacks, some FHM patients can have atypical severe attacks with signs of diffuse encephalopathy, confusion or impairment of consciousness (coma), prolonged hemiplegia lasting several days and in few cases seizures. Moreover, about 20% of FHM families show permanent cerebellar symptoms consisting of progressive cerebellar ataxia with or without nystagmus. Emotional stress and minor head trauma are among the most common triggers of FHM attacks (Pietrobon, 2007).

Common forms of migraine show multifactorial polygenic inheritance, but the causative genes of each type of FHM has been identified (Pietrobon and Striessnig, 2003): type 1 (FHM1, up to 50% of cases), type 2 (FHM2, from 20% to 30% of the cases) and type 3 (FHM3). These three types of FHM display similar symptoms with the exception of FHM1 that is uniquely associated with cerebellar symptoms (Pietrobon, 2007).

FHM1 is caused by mutations in the CACNA1A gene, in the chromosome 19p13, which codifies for the α_1 subunit of voltage-dependent $Ca_V2.1$ Ca^{2+} channels (see section 1.6). FHM1 shows an incomplete penetrance and other genetic or environmental factors could explain symptoms variability between subjects affected by the same FHM1 mutation. Episodic ataxia type 2 (EA2), spinocerebellae ataxia type 6 (SCA6) and certain cases of absence of epilepsy are other autosomal dominant neurological diseases caused by spontaneous mutations in the gene CACNA1A encoding for $Ca_V2.1$ Ca^{2+} channels (Pietrobon, 2005b).

FHM2 is caused to mutations in the ATP1A2 gene encoding for the α_2 subunit of the Na^+/K^+-ATPase located in the chromosome 1q23. The Na^+/K^+-ATPase is a P-type ion pump that utilizes the energy of ATP to actively transport Na^+ ions out of and K^+ ions into the cell generating the ion gradients that maintain the resting membrane potential

and cell volume and providing the driving force for nutrient and neurotransmitter uptake (Pietrobon, 2007). Na^+/K^+-ATPases are expressed in glial and neuronal cells where they play an important role in clearance of K+ from the extracellular space during neuronal activity and are fundamental for the clearance of glutamate released from the synaptic cleft. The active transport of glutamate into astrocytes and neurons is driven by both Na^+ and K^+ gradients. The α_2 isoform is expressed in neurons during embryonic development until birth and in glial cells after development (Pietrobon, 2005a)

FHM3 is caused by mutations in SCN1A; this gene in the chromosome 2q24 encodes for the α_1 subunit of the voltage-gated Na^+ channel $Na_V1.1$ identified in 2005. $Na_V1.1$ channels are primarly expressed in the central nervous system (CNS) during late postnatal stages, more in caudal than rostral regions. In particular they are highly expressed in inhibitory interneurons (Catterall et al., 2011). The FHM3 mutation (Gln1489Lys) accelerates the recovery from fast inactivation of recombinant human $Na_V1.5$ channels expressed in tsA201 cells, with a predictable increase in neuronal firing rates (Pietrobon, 2007).

1.4 Voltage-gated calcium channels

Voltage-gated calcium channels play a dominant role in the metabolism and physiology of excitable and non-excitable cells acting as key signal transducer from electrical signals of depolarization to chemical signals.

In skeletal, cardiac and smooth muscle cells Ca^{2+} entry mediated by voltage-gated channels initiate contraction directly or indirectly, by activation of Ca^{2+}-dependent Ca^{2+} release from sarcoplasmic reticulum. In the endocrine cells Ca^{2+} influx through voltage-gated channels initiate hormone secretion (Catterall, 2011). In central nervous system, voltage-gated calcium channels are involved many Ca^{2+}-dependent processes such as differentiation, synaptogenesis, neurite outgrowth, neuronal survival, activity dependent gene expression, plasticity, neuronal excitability and neurotransmitter release (Pietrobon, 2005b).

1.4.1 Structure of voltage-gated Ca^{2+} channels

The voltage-gated Ca^{2+} channels are members of a superfamily of transmembrane ion channel proteins that include voltage-gated potassium (K^+) and sodium (Na^+) channels (Catterall, 2011). They are proteins composed of the pore-forming and voltage sensing α_1 subunit and auxiliary subunits such as the β, $\alpha_2\delta$ subunit complex and sometimes a γ subunit (figure 1.2). The α_1 subunit is the main subunit (190 to 250 kDa) and constitutes the conduction pore. The voltage sensor, the gating apparatus and most of the known sites of channel regulation by second messengers, drugs and toxins are located within this subunit (Catterall et al., 2005).

The secondary structure of the α_1 subunit (composed by 2000 amino acid residues) is organized in four repeated homologous domains (I-IV) each one containing six transmembrane segments (S1-S6) of α helices. The S4 segment play a crucial role in voltage sensing and the membrane-associated pore loop between the segments S5 and S6 of each domain determines the selectivity and conductance of the channel (Catterall et al., 2005).

The β subunit is an intracellular hydrophilic protein of 50-65 kDa without transmembrane segments encoded by four genes. The $\alpha_2\delta$ subunit is a transmembrane disulfide-linked dimer of 170 kDa encoded by a single gene (four genes are known) and post-translationally cleaved. The mature α_2 is an extracellular protein and linked through disulfide linkage to the transmembrane δ subunits.

The γ subunit (33 kDa) is a glycoprotein with four transmembrane segments. It has been found in skeletal muscle Ca^{2+} channels, and related subunits are also present in brain and heart (Catterall, 2011).

The most variability of electrophysiological and pharmacological properties of Ca^{2+} channels arises primarily from the existence of at least 10 genes encoding for different α subunits with different splice variants of each subunit. In addition, further variability is due to different combinations with auxiliary subunits which are also subject to alternative splicing to yield additional isoforms (Catterall et al., 2005).

Ca^{2+} channel can be divided in three families on the basis of homology between the different amino acids sequence of α subunit: the identity is larger than 70% within a subfamily but less than 40% among the three family. The sequence identity increases if the pore loops and membrane spanning segments between S5 and S6 are compared (figure 1.2).

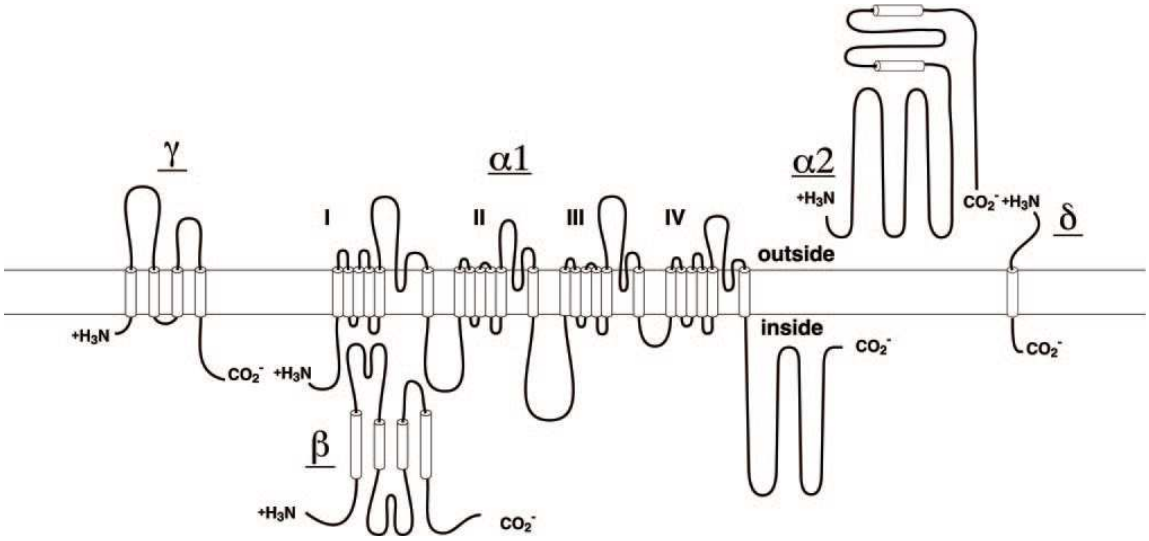

Figure 1.2. Structure and subunit composition of calcium Ca_v1 channel purified from skeletal muscle from figure 1 of Catterall (2011).

Cilinders represented in the model are α helices.

On the basis of electrophysiological and pharmacological properties of Ca^{2+} currents recorded in different cell types, Ca^{2+} channels have been divided in two main groups. depending on the voltage dependence of activation: low voltage activated (LVA) and high voltage activated (HVA) (Catterall, 2011). LVA channels, also referred as Ca_V3 channels (Ertel et al., 2000), are characterized by small single channel conductance with Ca^{2+} currents that are activated at negative potentials, inactivate rapidly and deactivate slowly. They are also called T-type Ca^{2+} channels for their transient openings.

HVA channels exhibit higher voltage of activation than LVA channels and Ca^{2+} currents that are characterized by larger single channel conductance and slower voltage dependent inactivation. Depending on the pharmacological responses to specific toxins HVA Ca^{2+} channels have been divided in four groups.

L-type Ca^{2+} channels are blocked by dihydropyridines, phenylalkylamines, and benzothiazepines and show the highest voltage activation and largest conductance with Ca^{2+} currents. Based on structural and functional classification they are also called Ca_V1 channels (Ertel et al., 2000).

The other groups of Ca^{2+} channels have intermediate properties between L-type and T-type Ca^{2+} channels and are inhibited by different toxins.

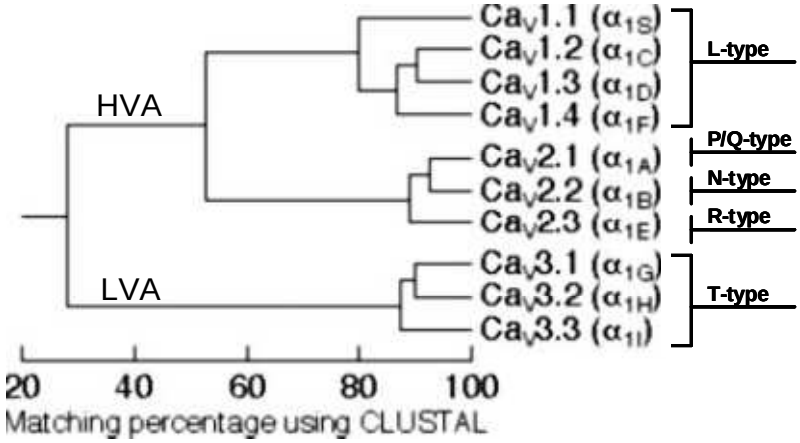

Figure 1.3 Phylogenetic representation of the primary sequences of the Ca^{2+} channels.

All sequence pairs were compared and clearly define three subfamilies with intrafamily sequence identities above 80 % (Ca_V1, Ca_V2, and Ca_V3). A consensus sequence was defined for each subfamily, and these three sequences were compared to one another, with intersubfamily sequence identities of ~ 52 % (Ca_V1 versus Ca_V2) and 28 % (Ca_V3 versus Ca_V1 or Ca_V2).

Figure modified by Catterall et al., 2005.

N-type Ca^{2+} channels are specifically and irreversibly blocked by ω-conotoxin GVIA (ω-CgTxGVIA) from the venom of the *Conus geographus* snail. The usage of a pharmacological blocker allowed to isolate N-type Ca^{2+} currents which are very different in terms of kinetics and voltage dependence depending on the type of neurons recorded.

P/Q-type Ca^{2+} channels are specifically and irreversibly blocked by ω-agatoxin IVA (ω-AgaVIA) from the venom of the *Agelenopis aperta* spider and by ω-conotoxin MVIIC (ω-CTx-MVIIC) from *Conus magus* snail that however blocks reversibly also the N-type Ca^{2+} channels.

R-type Ca^{2+} channels are resistant to most subtype-specific organic and peptide Ca^{2+} channel blocker with the exception of the peptide SNX-482 derived from *Hysterocrates gigas* spider that is a specific blocker of some R-type Ca^{2+} channels isoforms (Catterall, 2011). Mammal neuronal cells express different isoforms of R-type Ca^{2+} channels the majority of them are sensitive (with different affinity) to SNX-482 (Tottene et al., 2000).

Based on structural and functional classification P/Q, N-, R-type Ca^{2+} channels are named $Ca_V2.1$, $Ca_V2.2$ and $Ca_V2.3$ channels respectively (Ertel et al., 2000).

1.4.2 Ca^{2+} channels localization and function

All the different Ca_V channels, except $Ca_V1.1$, are expressed in the brain, with a differential distribution within different neuronal populations and different localization within the same neuron. Different splice variants of a given subunit are also differentially distributed and localized in the brain. In particular $Ca_V1.1$ are expressed in the transverse tubules of the skeletal muscles.

$Ca_V1.2$ channels are localized in cardiac and smooth muscles, in the soma and proximal dendrites of neurons and endocrine cells.

$Ca_V1.3$ channels are expressed in sensory cells (such as photoreceptors or cochlear hair cells), in endocrine cells. A small percentage of Cav1.3 is also present in the heart, vascular smooth muscle and in the soma and proximal dendrites of neurons.

$Ca_V1.4$ channels are expressed in retinal cells (photoreceptors and bipolar cells), spinal cord and lymphoid tissue. Ca_V1 channels are involved in different physiological processes: they initiate contraction and secretion in muscle and endocrine cells, govern vesicle fusion and subsequent neurotransmitter release from cochlear inner hair cells for the hearing in the cochlea, regulate pacemaker activity in the heart; mediate neuronal excitability and gene expression within the brain (Catterall et al., 2005).

The Ca_V3 Ca^{2+} channels have been localized predominantly within the somatic and dendritic compartments of cerebral cortex, amygdale and thalamus (where they are involved in thalamic oscillations). Additionally they are expressed in the placenta, ovary and heart ($Ca_V3.1$) and in kidney, liver, smooth muscle ($Ca_V3.2$) (Catterall et al., 2005)

$Ca_V2.1$, $Ca_V2.2$ and $Ca_V2.3$ channels are mostly expressed in neurons. At presynaptic terminals they are involved in initiating action potential (AP)-evoked neurotransmitter release at most fast synapses whereas at dendrites and soma they are involved in neuronal excitability (Pietrobon, 2007; Catterall et al., 2005).

$Ca_V2.1$ channels are expressed in all the brain structures involved in the pathogenesis of migraine such as trigeminal ganglia, cerebral cortex and in the brainstem nuclei involved in nociception control (Pietrobon and Striessnig, 2003)

1.4.3 Presynaptic Ca^{2+} channels controlling neurotransmission

Transmitter release at central synapses is triggered by brief and local transients of Ca^{2+} influx (up to 100 µM) through voltage–gated Ca^{2+} channels. However amplitudes and duration of Ca^{2+} transients can vary a lot depending on the type of the synapse studied. In the calyx of Held synapse, for example, small (10-25 µM) local Ca^{2+} signals of less than 1 ms of duration are sufficient to trigger neurotransmitter release at the terminal (Schneggenburger and Neher, 2005).

Voltage-gated Ca^{2+} channels are located in close proximity to the Ca^{2+} sensors on readily releasable vesicles through specific interactions with multiple proteins of the active zones such as SNAREs, RIM and scaffolding proteins (Catterall and Few, 2008).

N-, P/Q- and R-type Ca^{2+} channels usually cooperate in initiating synaptic transmission at a given synapses but their contribution can be different at different synapses. There are strong evidences that a different contribution of different Ca^{2+} channels in controlling neurotransmitter release can be due not only to differences in their kinetics properties but also to differences in their subcellular distribution within the presynaptic terminals (Wu et al., 1999). Moreover it has been shown that Ca^{2+} channels are not uniformly distributed across presynaptic terminals that arise from the same axon (Reid et al., 2003).

Excitatory synaptic transmission at cerebral pyramidal cell synapses depends predominantly on P/Q-type Ca^{2+} channels in different brain. An example can be found in the cortex where the connections between pyramidal cells and fast spiking (FS) interneurons in layer 2/3 somatosensory and layer 5 motor cortex, are regulated by P/Q-type Ca^{2+} channels (Pietrobon, 2010a; Ali and Nelson, 2006; Tottene et al., 2009; Zaitsev et al., 2007; Rozov et al., 2001). By contrast, synapses between layer 5 pyramidal cells and burst-firing bipolar interneurons of motor cortex, strongly depend on N-type Ca^{2+} channels (Ali and Nelson, 2006).

Because of the wide heterogeneity between interneurons, Ca^{2+} channels initiating inhibitory neurotransmission in the cortex are relatively unknown. For example synapses between FS interneurons and pyramidal cells in layer 5 motor and layer 2/3 prefrontal cortex of rats are totally mediated by P/Q-type Ca^{2+} channels (Ali and Nelson, 2006, Zaitsev et al., 2007), but with the exception of layer 5 of the motor cortex, where it was exclusively dependent on N-type Ca^{2+} channels (Ali and Nelson, 2006).

1.5 Synaptic plasticity

The strength of synaptic transmission can vary enormously depending on activity-dependent pre- or postsynaptic modifications which can alter the response properties of a single synapse. Activity-dependent changes in synaptic transmission arise from a large number of mechanisms known as synaptic plasticity (Catterall and Few 2008, Abbot and Regehr, 2004; Zucker and Regehr 2002). Plasticity in synaptic transmission in turn modify the neural network patterns of activity and informational processes between neurons. These modifications can last from milliseconds to months.

One type of plasticity, short-term plasticity, occurs on a timescale of millisecond for at most few minutes allowing synapses to perform critical computational functions within neural circuits. This plasticity can result in synaptic enhancement throughout three processes that vary in terms of durations: facilitation, augmentation and post-tetanic potentiation (PTP). The molecular mechanisms mediating various forms of short-term plasticity are still under debate but all of these forms are Ca^{2+}-dependent.

Short term plasticity can also induce a reduction in neurotransmitter release resulting in short term depression (Catterall and Few, 2008; Zucker and Regehr, 2002). These processes are often overlapped at the same synapse and it can be difficult to separate different components of short term plasticity.

Facilitation lasts less than a second. It can been observed with pairs of stimuli in which the second post-synaptic potential or post-synaptic current (PSP or PSC respectively) can be up to five times the amplitude of the PSP or PSC elicited by the first presynaptic action potential. During brief trains of action potentials (APs), successive PSPs or PSCs increase in terms of amplitude which can reach several times of the amplitude of PSP or PSC elicited by the first AP of the train. Facilitation often builds and decays with a time course with an exponential of approximately 100 ms (figure 1.4; Zucker and Regehr, 2002).

With long train of APs, other processes become increasingly important. The synaptic strength enhanced by a single AP is low (1-15%); however when many AP are delivered within a train that can last seconds or minutes, the overall effect is a many-fold enhancement. When the process of enhancements grows and decays with a time costant of 5-10 s, it's usually known as augmentation. This is different from PTP which lasts from 30s to several minutes (Figure 1.4; Zucker and Regehr, 2002).

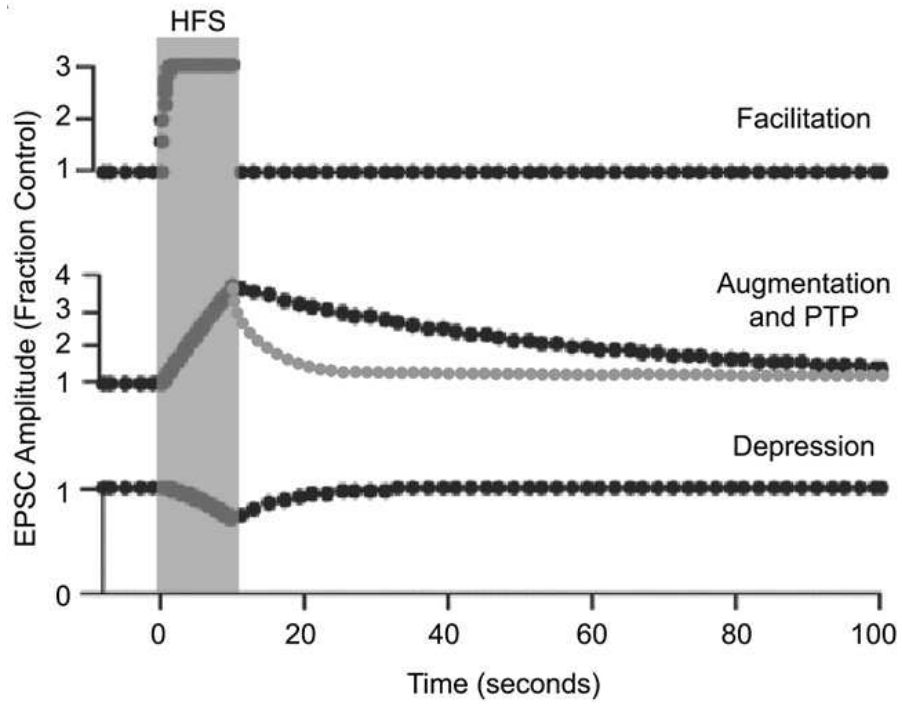

Figure 1.4. Multiple forms of short-term plasticity from Catterall and Few (2008).
Simulated experiment showing the relative rise and decay times for multiple forms of short-term synaptic plasticity during and following high frequency stimulation (HFS). Excitatory postsynaptic currents were evoked at 0.5 Hz versus time with tetanic stimulation (HFS 10 Hz for 10 s) beginning at time 0.

Many mechanisms may lead to facilitation of synaptic plasticity; the most common molecular mechanism involve the residual Ca^{2+} remaining in the synapse after an AP which can enhance synaptic transmission. This model is supported by the fact that application of the slow Ca^{2+} chelator ethylene glycol-bis(β-amionoethyl ether)-N,N,N',N-tetraacetic acid (EGTA) in the presynaptic terminal reduces short term enhancement as proposed by Katz and Miledi in 1968 (Catterall and Few, 2008; Zucker and Regehr, 2002). The simplest explanation is represented by the binding of the residual Ca^{2+} present in terminal to the Ca^{2+} sensor for exocytosis which in turn would lead to an increase in the neurotransmitter release. More recent data suggest that the residual Ca^{2+} triggers an increase in synaptic transmission by acting indirectly another Ca^{2+}-binding protein(s) (Catterall and Few, 2008). For example, it has been suggested that the binding of the residual Ca^{2+} to another Ca^{2+} sensor could increase the release probability. This facilitating sensor can act by increasing the entry of Ca^{2+} during the following AP or by directly modulating the vesicular release machinery and therefore enhancing the neurotransmission. Otherwise there is evidence that at particular synapses the mechanism of synaptic facilitation proposed involves a partial saturation of high-

affinity presynaptic Ca^{2+} buffers (parvalbumin, calbindin-D28K for example) by the residual Ca^{2+} remaining after an AP. In presence of a second AP close to the first one, more of the entering Ca^{2+} remains free and available to act on the normal Ca^{2+} sensor for neurotransmitter release. (Catterall and Few, 2008; Zucker and Regehr, 2002).

Augmentation is mostly caused by an increase in the release probability of vesicle. Augmentation and PTP are overlapping physiological processes. The rate of Ca^{2+} clearance from the synapse can determine which one of the two processes may occur.

Residual Ca^{2+} accumulated during sustained stimulation that induces augmentation and PTP is eliminated from the synapse by the Na+/Ca^{2+} exchanger and the Ca^{2+}-ATPase.

Long trains of APs increase intracellular Ca^{2+} and Na^{+} concentrations and slow down the rate of Ca^{2+} clearance by Na^{+}/Ca^{2+} exchange. Residual Ca^{2+} driving PTP can also result from the slow efflux from mitochondrial or endoplasmic reticulum Ca^{2+} accumulated during tetanic stimulation.

At many synapses trains of AP or closely paired stimuli can reduce the synaptic strength indicating the presence of short term depression. Many mechanisms can contribute to this type of synaptic plasticity. The most common one is represented by the depletion of the ready releasable pool of vesicles which in turn would produce a decrease in neurotransmitter release. Reduced strength in synaptic transmission can also be caused by the release of modulatory substances from the activated presynaptic terminals or postsynaptic cells which, for example, can activate G-protein-coupled receptors located on the presynaptic terminals, or neighboring cells (also glial cells can be involved in some forms of short term plasticity). Finally, postsynaptic properties such as desensitization of ligand-gated receptors can make the target neuron less sensitive to neurotransmitter (Catterall and Few, 2008; Zucker and Regehr, 2002).

There are many sites of regulation of short-term plasticity such as AP waveform, calcium channels or postsynaptic release of neuromodulators (figure1.5) and many mechanisms can contribute to enhancement or depression of neurotransmission even if their roles remain under debate.

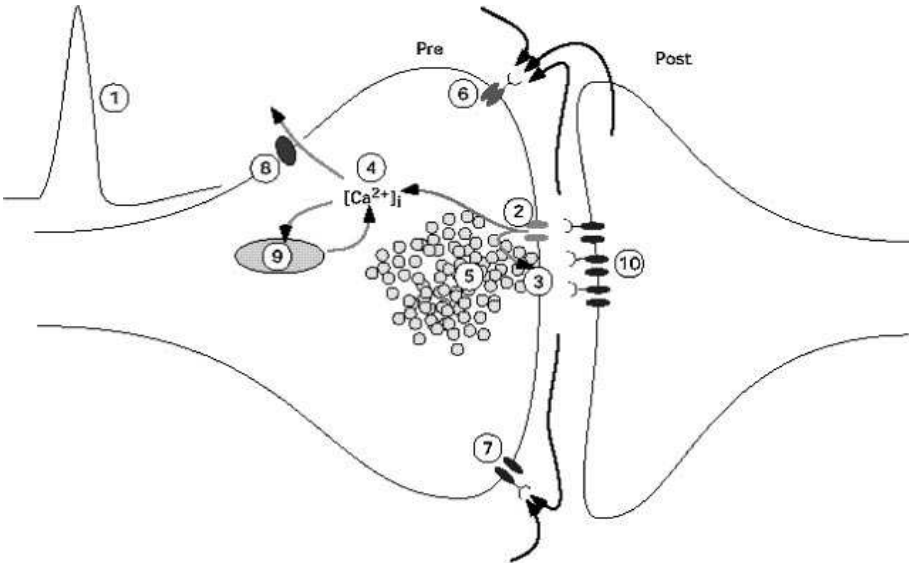

Figure 1.5. Sites of regulation of short-term synaptic plasticity from Zucker and Regehr (2002).
(1) AP waveform, (2) Ca^{2+} channel activation, (3) facilitation trigger and the readily releasable pool, (4) residual intracellular Ca^{2+} ($[Ca^{2+}]i$), (5) reserve pool, (6) metabotropic autoreceptors, (7) ionotropic autoreceptors, (8) Ca^{2+}-ATPase, regulating residual [Ca2C]i in augmentation, (9) mitochondrial regulation of residual $[Ca^{2+}]i$ in PTP, (10) postsynaptic receptor desensitization.

1.6 Functional consequences of FHM1 mutations

All the 21 FHM1 mutations (figure 1.6) are missense mutations that produce substitutions of conserved amino acids in important functional regions of the $Ca_V2.1$ channel including the voltage sensor and the pore lining. (Pietrobon, 2010b).

The functional consequences of 13 FHM1 mutations have been investigated in heterologous expression systems expressing recombinant $Ca_V2.1$ Ca^{2+} channels. The expression of $Ca_V2.1$ is almost entirely restricted to neuronal cells, five of these mutations were therefore studied in neurons from $Ca_V2.1$-/- mice expressing human $Ca_V2.1$ α_1 subunit (Tottene et al., 2002).

Studies on heterologous expression systems (mammalian cell line: human embryonic kidney, HEK293) showed that the FHM1 mutations alter many biophysical properties of $Ca_V2.1$ channels and in some cases different mutations can lead to different effects. Studies of single channel properties in eight different mutations showed an enhanced Ca^{2+} influx in a wide range of depolarizations as a consequence of an increased channel open probability.

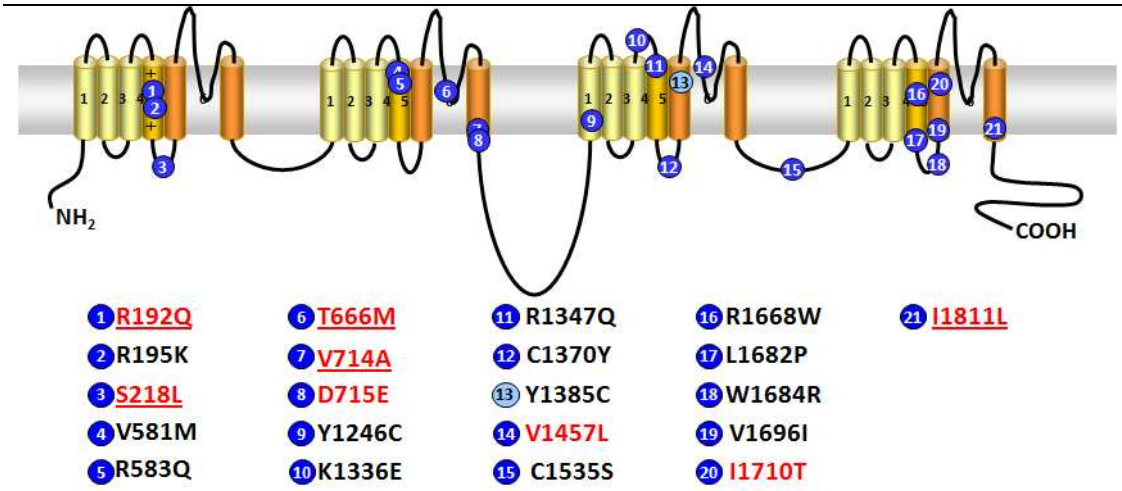

Figure 1.6. Secondary structure of α1 subunit of CaV2.1 Ca^{2+} channels and localization of FHM1 mutations from Pietrobon (2010b).

Functional consequences of eight mutations on recombinant CaV2.1 have been studied in heterologous expression systems (highlited in red); the underlined FHM1 mutations have been studied also in neurons of CaV2.1 -/- expressing human Cav2.1 α1 subunits.

Y1385C mutation (13) is a sporadic mutation.

This increase is mainly caused by a shift to lower voltages of the channel activation curve which elicits a Ca^{2+} influx through the mutant channels in response to small depolarizations insufficient to open wild type (WT) channels (Pietrobon, 2010b; van den Maagdenberg et al., 2004; Tottene et al.,2002).

In 2004 van den Maagdenberg et al. reported the generation of a knock-in (KI) mouse model obtained by introducing the human R192Q FHM1 mutation at the corresponding position in the mouse orthologous *cacna1a* gene by homologous recombination. The creation of this KI mouse allowed the study of the mutated Ca^{2+} channel in neurons at the endogenous level of expression.

The mutation consists in the substitution of a positively charged arginine with a neutral, non polar glutamine in the S4 segment of domain I, which forms part of the voltage sensor of the channel.

The homozygous R192Q (RQ/RQ) KI mice are healthy animals and do not exhibit an overt phenotype. Recordings from cerebellar granule cells in primary culture showed a larger whole-cell $Ca_V2.1$ currents in RQ/RQ KI mice than in WT mice within a broad voltage range of voltages (figure 1.7). Mutant $Ca_V2.1$ channels activated at 8-9 mV more negative voltages than the corresponding WT channels. At high voltages where the open probabilities were maximal CaV2.1 currents are similar between KI and WT suggesting that the R192Q mutation doesn't alter the functional $Ca_V2.1$ channel. The

mutation also affects the kinetics of activation of CaV2.1 channels as they are faster in KI mice than in WT (van den Maagdenberg et al., 2004).

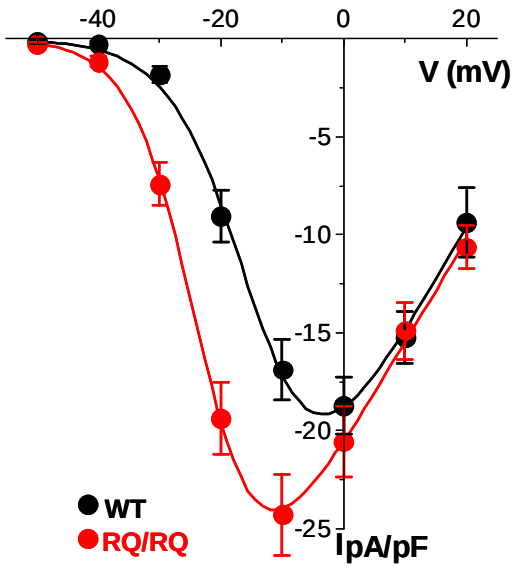

Figure 1.7. $Ca_V2.1$ current density (I) as a function of the voltage from cerebellar granule of R192Q KI and WT mice from van den Maagdenberg et al (2004).

In vivo experiments have demonstrated that R192Q KI mice are more susceptible to the induction of CSD than WT mice. Following visual cortex stimulation, KI mice show a lower threshold for CSD induction and an increased velocity of CSD propagation (van den Maagdenberg, 2004). This finding strengthens the view that CSD plays a crucial role in the pathogenesis of migraine and suggests a key role of $Ca_V2.1$ channels in the initiation and propagation of CSD.

Tottene et al. (2009) have shown that the gain-of-function of $Ca_V2.1$ channel enhances glutamate release due to increased action potential-evoked calcium influx through $Ca_V2.1$ channels at cortical pyramidal cells autapses in microculture and acute slices of primary somatosensory cortex of R192Q KI mice. This increase in glutamate release may explain the facilitation of experimental CSD in FHM1 mutant mice. In fact induction and propagation of CSD in KI mice can be rescued to WT values when glutamate release at pyramidal cell synapses is brought back to WT values by applying sub-saturating concentration of ω-agatoxin IVA (Tottene et al., 2009).

Tottene et al. (2009) propose a model of generation of CSD in which activation of presynaptic voltage-gated Ca^{2+} channels (in particular P/Q-type) with consequent release of glutamate from recurrent cortical pyramidal cell synapses and activation of NMDA receptors are key components for induction of CSD.

Sufficiently intense stimuli may lead anomalous increase in the extracellular concentration of K^+ ions and a sustained neuronal depolarization accompanied by an increase in neuronal firing. CSD ignition occurs when the regulatory mechanisms that normally keep the extracellular K^+ concentration $[K^+]_o$ within the physiological range are overwhelmed by the build-up of $[K^+]_o$ via a positive feedback cycle that makes self-regenerating the initially gradual neuronal depolarization; this positive feedback cycle initiates when a sufficient number of V-dependent and/or $[K^+]_o$-dependent cationic channels are activated to generate a net sustained inward current, with consequent further depolarization and further increase of the local $[K^+]_o$, leading to further activation of the cationic channels (Pietrobon, 2007; Somjen, 2001). The nature of these cationic channels remains unclear and controversial (Somjen, 2001), although there is strong pharmacological support for a key role of NMDA receptors, as NMDA receptors antagonists inhibit, in vivo, CSD induction and propagation in a dose-dependent manner (Pietrobon, 2005, 2007). Moreover there is clear evidence that CSD initiates and propagates at the level of the dendrites of pyramidal cells (Pietrobon, 2007; Somjen, 2001) and involves an increased conductance in specific dendritic subregions (Canals et al., 2005). Also controversial is the mechanism of CSD propagation. Among the hypotheses: interstitial K^+ diffusion initiating in adjacent dendrites the positive feedback cycle that ignites CSD or CSD propagation through gap junctions (Somjen, 2001)

Tottene et al (2009) studied the neurotransmission between connected pairs of layer 2/3 pyramidal cells and multipolar fast-spiking (FS) interneurons that mediate perisomatic inhibition in acute slices of somatosensory cortex. This study showed that excitatory neurotransmission at PYR-FS synapses is increased in R192Q KI versus WT whereas inhibitory neurotransmission at FS interneuron-pyramidal synapses is unaltered in KI mice. Even though synaptic transmission is mediated by P/Q-type Ca^{2+} channels at both excitatory and inhibitory synapses. These findings demonstrate that FHM1 mutations may differently affect synaptic transmission and short-term plasticity at different cortical synapses, and, as a consequence, very likely alter the neuronal circuits that coordinate and dynamically adjust the balance between excitation and inhibition during cortical activity (Tottene et al., 2009).

Functional alterations in these circuits may underlie the abnormal processing of sensory information of migraineurs in the interictal period suggesting a vulnerability of the cortex to ignition of CSD in response to migraine triggers such as intense, repetitive sensory stimulation.

1.7 Organization of the cortex

The cerebral cortex is characterized by a double organization defined by layer and columns. The most typical form of neocortex contains six layers numbered from the outer surface (*pia mater*) of the cortex to the inner white matter (Kandel, 2000). The laminar organization can be different at functionally different cortices.

Layer 1 (molecular layer) is characterized by few cell bodies and is mainly occupied by dendrites and axons of cells located in deeper layers.

Layer 2 (external granule cells layer) is characterized by round-shaped cells and in mouse cortex is fused with the layer 3 (external pyramidal layer) which contains several types of neurons, in particular pyramidal cells. Layer 4 is the internal granule cell layer populated by granule cells which are the principal recipient layer for thalamocortical inputs. The thalamocortical inputs are in turn transmitted from granule cells to layers 2, 3, 5 and 6 (de Kock et al., 2007). Layer 5 is the internal pyramidal layer characterized by the presence of pyramidal cells. These cells are bigger than pyramidal cells located in layer 2/3. Layer 5 pyramidal neurons project their axons to subcortical regions and constitute the principal cortical output to excite other cortical areas. Layer 6 is the polymorphic or multiform layer because is occupied by several types of neurons. Together with the layer 5, they project back to the thalamus regulating thalamocortical interactions (de Kock et al., 2007).

Cortical neurons are also organized in vertical columns that contains all six cortical layers. The neuronal network within a cortical column performs basic signal transformations of input; in particular in somatosensory cortex each functional columns is defined by discrete and well-defined structure in layer 4 known as barrel. These layer 4 barrels are arranged somatotopically in an almost identical fashion to the layout of the whiskers in the snout (Petersen, 2007). The primary somatosensory cortex processes the information from mouse vibrissae.

1.8 Cellular populations in the cortex

Neurons in the cortex can be divided in two principal groups: pyramidal cells which constitutes the biggest population within the cortex and interneurons which represent 20-25% of the neurons in the neocortex.

In the normal cerebral cortex pyramidal neurons contacts make excitatory synapses releasing the neurotransmitter glutamate onto other pyramidal neurons generating a positive feedback. Different subtypes of inhibitory interneurons play a crucial role preventing over-excitation and contributing to maintain the balance between excitation and inhibition.

The interactions between GABAergic interneurons and glutamatergic principal cells are reciprocal: interneurons inhibit principal cells and are excited by them. In fact the connectivity between these two neuronal classes is quite high: individual interneurons can inhibit >50% of principal cells located within ~100 µm and receive excitatory input from a large fraction of them (Kapfer et al., 2007; Silberberg and Markram, 2007). Thus, not only are GABAergic interneurons excited in proportion to the level of local network activity, but they directly influence it through their inhibitory feedback. This simple connectivity pattern is ubiquitous in cortex and forms the basis for so-called feedback or recurrent inhibition (Figure 1.8). Of course, not all cortical excitation received by inhibitory interneurons is locally generated. Interneurons can receive excitatory inputs from other pyramidal neurons on which they don't make inhibitory synapses generating feedforward inhibitory circuits. Together, these two simple inhibitory circuits, feedback and feedforward, represent fundamental building blocks of cortical architecture and account for the fact that cortical excitation and inhibition are inseparable (figure 1.8) (Isaacson and Scanziani 2011).

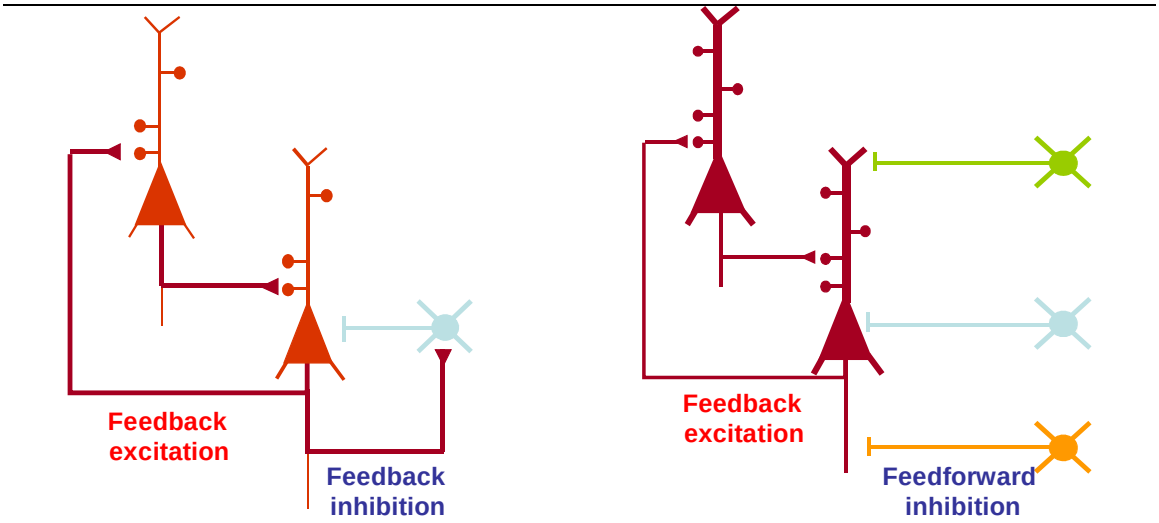

Figure 1.8. Schematic representation of cortical circuits.

Triangle-shaped soma represent pyramidal cells and circles represent interneurons. Pyramidal cells mediate excitatory synapse onto other pyramidal cells and several types of interneurons which make inhibitory synapses onto pyramidal cells at different positions (soma, dendrites and axons).

Interneurons can be classified through morphological parameters regarding their axonal arborization and consequnently their postsynaptic targets. In fact different types of inhibitory interneurons, which release the neurotransmitter GABA, inhibit distinct compartments of principal neurons (Silbeberg and Markram, 2007; Markram et al., 2004). Interneurons can also be classified based on their intrinsic electrophysiological properties and protein expression markers (Isaacson and Scanziani, 2011; Kawaguchi and Kondo, 2002).

Because of the many parameters that can be used to describe interneurons and given the vast amount of data vailable on these cells, it has recently been proposed an unequivocal terminology to classify these cells based on morphological, electrophysiological and marker expression features (The Petilla Interneuron Nomenclature Group, 2008).

Two subtypes of interneurons involved in polysynaptic inhibitory circuits which are involved in the maintenance of excitation-inhibition balance are fast-spiking interneurons (FS) and martinotti cells (MC).

FS interneurons show a basket cell morphology and represent about 50% of all inhibitory interneurons. They make synapses onto soma and proximal dendrites of pyramidal cells which places them in a unique position to adjust the gain of the integrated synaptic response (Markram et al., 2004).

MCs are distinguished from other interneurons by their axonal harborization which is characterized by axonal projections with a horizontal spread in layer I that typically extend beyond a column radius. Most MCs have a bitufted dendritic morphology and ovoid soma, but some MCs have multipolar dendritic morphology (Silbeberg and Markram, 2007; Markram et al., 2004; Wang et al., 2004).

These cells are particularly interesting because they receive facilitating excitatory synapses from pyramidal cells and make inhibitory synapses mainly onto dendrites of the pyramidal cells in layer 1 (Silbeberg and Markram, 2007; Kapfer et al., 2007; Silberberg, 2008).

Given the difficulty to find this type of interneuron in the mouse cortex, many transgenic mice have been created to overcome this problem.

In this thesis we take advantage of GIN (GFP Inhibitory Neurons) mice which express an enhanced GFP under the control of GAD67 promoter. GIN mice have been created by pronuclear microinjections of transgene DNA into one-cell stage embryos. The transgene contruct is integrated randomly in the mouse genome therefore the transgene expression is influenced by the positional effect influences. Although the promoter is

expressed by all GABAergic neurons, cortical GFP expression is restricted to somatostatin-positive (SOM^+) interneurons (Oliva et al., 2000).

GIN interneurons represent a variable percentage of SOM^+ neurons depending on cortical layer and area: in the mouse primary somatosensory cortex GIN neurons constitute from 35% to 53% of the SOM+ population (Ma et al., 2006; Xu et al., 2006). Axonal branching reconstructions indicate that most GIN neurons are Martinotti cells (Fanselow et al., 2008; Ma et al., 2006). GIN neurons show both multipolar and bitufted dendritic morphology, but the multipolar morphology prevails, thus indicating that they are a subpopulation of Martinotti cells (Halabinsky et al., 2006) (figure 1.9).

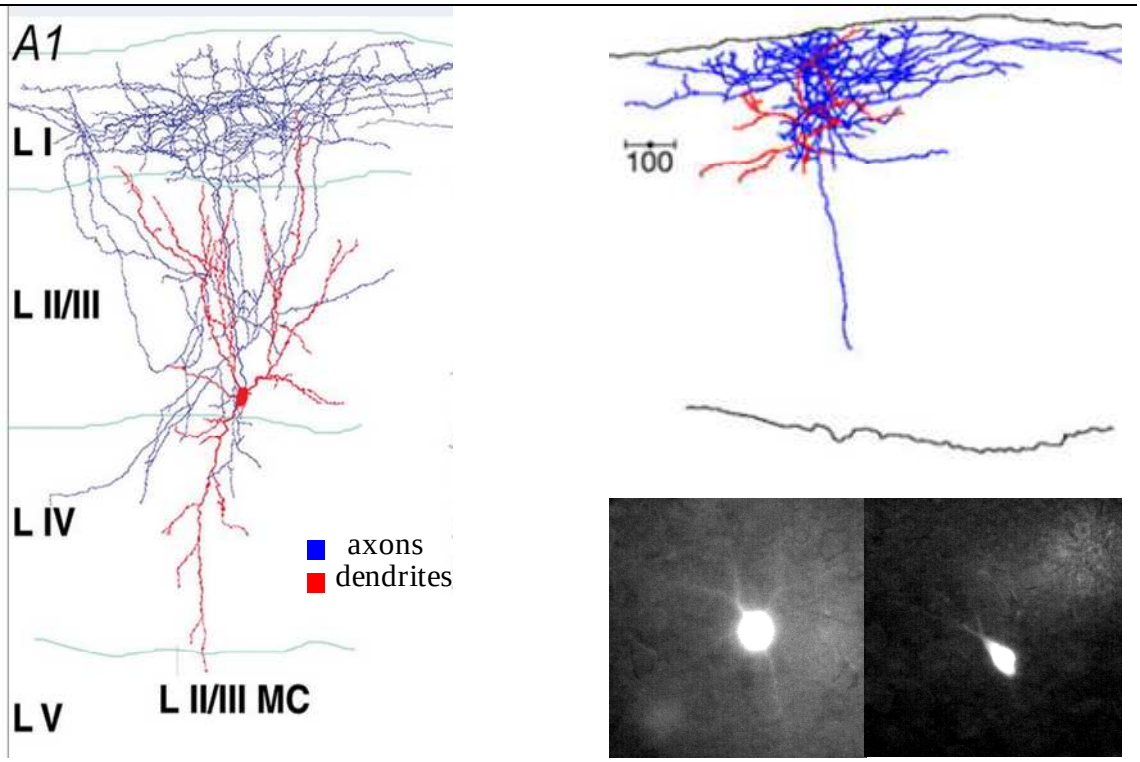

Figure 1.9. Axonal and dendritic reconstruction of a layer 2/3 Martinotti cells from rat cortex (on the left) and layer 2/3 SOM+ GFP+ interneuron from GIN mouse (on the right) obtained by Wang et al (2004) and McGarry et al (2010) respectively.

Down below two representative images of SOM+ interneurons from GIN mouse obtained in our laboratory.

1.9 Spontaneous cortical activity

Cerebral cortex is spontaneously active. Even during slow wave sleep, cortical and subcortical networks interact to generate rhythmic patterns of activity at different

frequencies such as slow rhythm characterized by slow oscillations (<1 Hz) that occurs during natural sleep and certain forms of anesthesia. These slow oscillations are characterized by synaptically mediated depolarizations that can be subthreshold or generates APs. These fluctuations are called up states. The up states are followed by a period of silence in which there's a diminution of synaptic inputs leading to the cessation of firing and the rescue of the membrane resting potential (down state) (Petersen et al., 2003; Sanchez-Vives and McCormick, 2000; Steriade et al., 1993).
Spontaneous slow oscillations similar to the ones observed *in vivo* have also been reported *in vitro* (figure 1.10). (Sanchez Vives and McCormick, 2000).
This finding shows that this activity can be maintain by cortical circuits in slices without corticothalamic interactions.

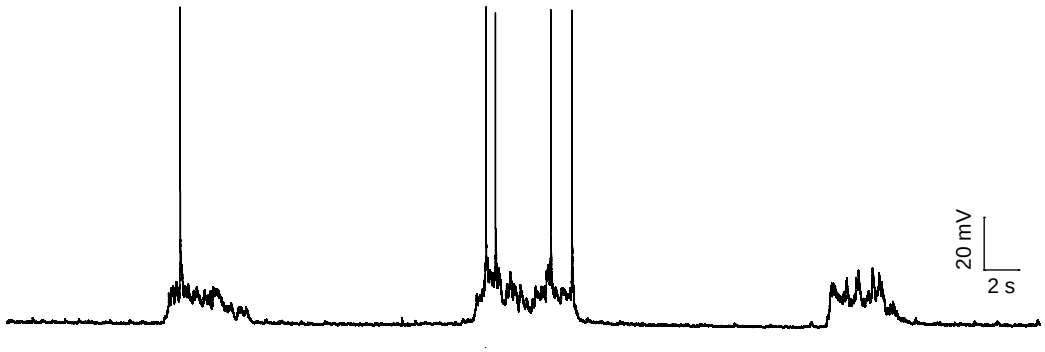

Figure 1.10. Typical current clamp recording of up-states from a layer 2/3 PYR cell of somatosensory cortex.
The AP firing is only localized during the depolarization of the membrane potential.

The mechanisms underlying the generation and maintenance of spontaneous activity of the up-states are still under debate but recent findings points towards an increasing importance of network recurrent activity (Shu et al., 2003). This spontaneous network activity originates within the cortex and propagates after to subcortical areas (e.g. thalamus and striate), as deducible from lesion experiments (Amzica and Steriade., 1995). Recent findings point to intrinsically active pacemaker neurons as spontaneous network activity generators: when a sufficient number of these neurons fire simultaneously, postsynaptic neurons are triggered to fire action potentials, recruiting in turn other connected neurons and "turning on" the cortical network (Bazhenov et al., 2002; Le Bon-Jego and Yuste, 2007).

2. AIMS OF WORK

The findings of different effects of the R192Q FHM1 mutation at excitatory and inhibitory synapses (Tottene et al., Neuron, 2009) suggest that episodic disruption of the excitation-inhibition balance may underlie the increased susceptibility to CSD found in knock-in (KI) mice. To further explore this working hypothesis it is important to investigate whether FHM1 mutations affect also other synapses of the brain cortical microcircuits and whether the finding of unaltered inhibitory neurotransmission is specific for fast-spiking (FS) interneuron synapses or is general and holds for other (or all) inhibitory synapses.

Another important inhibitory subcircuit in the cortex involves somatostin-expressing (SOM+) interneurons that mediate dendritic inhibition and receive facilitating excitatory synapses from pyramidal (PYR) cells. Voltage-gated calcium channels controlling the neurotransmitter release at both excitatory and inhibitory synapses of this inhibitory subcircuit are not known. We took advantage of transgenic mouse line (GFP-expressing interneurons, GIN) which expresses an enhanced form of GFP in a subpopulation of SOM^+ interneurons to establish whether P/Q-type Ca^{2+} channels are involved in controlling the neurotransmitter release at excitatory and reciprocal inhibitory connections between PYR cells and SOM^+ interneurons. If P/Q-type calcium channels are involved in the neurotransmitter release it will be interesting to study the effect of FHM1 mutations at these synapses in FHM1 KI mice crossbred with GIN mice.

Considering the specific polysynaptic inhibitory subcircuit studied in Tottene et al (2009), involving FS interneurons and PYR cells, the gain of function of glutamate release at the recurrent synapses between pyramidal cells would certainly increase network excitation; in contrast, the gain of function of glutamate release at the PYR-FS synapses would lead to enhanced recruitment of interneurons and enhanced inhibition. However, during high-frequency repetitive activity the enhanced recruitment of FS interneurons is expected to cease rapidly because the PC-FS synapses depress strongly during AP trains and short term depression is even stronger in KI mice (Tottene et al., 2009). This analysis, even though restricted to a specific subcircuit, indicates that the differential effects of FHM1 mutations on excitatory and inhibitory neurotransmission may produce overexcitation in certain brain conditions, but may leave the excitation-inhibition balance within physiological limits in others. To investigate whether FHM1 mutations might lead to an unbalance between excitation and inhibition towards

excitation I collaborated with Alessandra Fabbro in studying the excitatory and inhibitory synaptic charge received by a layer 2/3 PYR cell in WT and R192Q KI mice during ongoing network activity without any type of stimulation.

3. RESULTS

3.1 Characterization of excitatory and inhibitory connection between pyramidal cells and somatostatin interneurons in GIN mice

I performed dual patch clamp recordings from connected pairs of pyramidal (PYR) cells and SOM^+ interneurons of layer 2/3 of somatosensory cortex in thalamocortical GIN slice to study the excitatory connection onto these SOM^+ interneurons and reciprocal inhibitory connection. I applied saturating concentrations of specific calcium channels blocker to establish the involvement of calcium (Ca^{2+}) channels in controlling the neurotransmitter release at both excitatory and inhibitory synapses between PYR cells and SOM^+ interneurons.

During the presentation of the results I will call the fluorescent SOM^+ interneurons from GIN mice GIN interneurons.

GIN interneurons were recorgnized on the basis of their fluorescent emission; PYR cells (selected around the fluorescent interneuron) were recognized by their morphology and, when possible, by their firing properties at increasing amplitude of current injections.

3.1.1 Characterization of excitatory connection between PYR cells and GIN interneurons

In dual patch clamp experiments I elicited action potential (AP) in the presynaptic PYR cell with suprathreshold depolarizing current-injection pulses (7.5 ms duration) in current clamp (V=-70 mV). Once a connected pair was found, the synaptic response to a train of 5 APs at 25 Hz was recorded in the postsynaptic GIN interneuron (held at -70 mV in current clamp) for at least 30 consecutive trials at 15 s intervals.

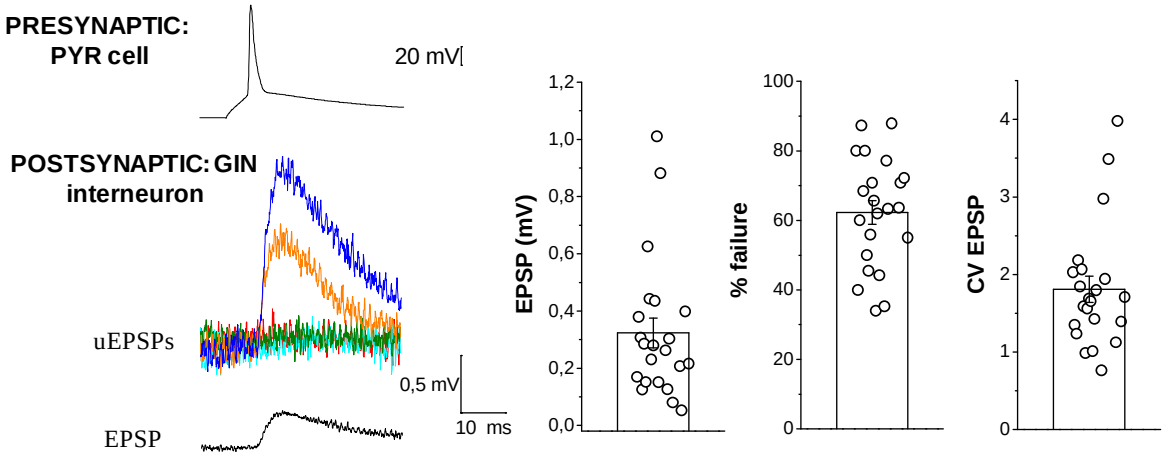

Figure 3.1. Biophysical properties of excitatory synaptic connection between PYR cell and GIN interneurons.

On the left in the upper part: representation of the first AP of the train of five AP elicited in the presynaptic PYR cell; in the middle part five representative unitary EPSPs (uEPSPs) induced by the first presynaptic AP of consecutive trials and down below mean uEPSP (EPSP) obtained by averaging several uEPSPs of consecutive trials including the failures.

On the right: histograms of EPSP, percentage of failure and the coefficient of variation of the first response recorded from 22 unitary connections.

I characterized the unitary postsynaptic potentials (uEPSPs) elicited in the postsynaptic GIN interneuron by single APs in terms of mean amplitude, percentage of failures and coefficient of variation (figure 1).

The mean amplitude of uEPSP (EPSP) was obtained by averaging uEPSPs including the failures produced by at least 30 consecutive trials at 15s interval (0.32 $\pm$ 0.05 mV; n=22).

The percentage of failures represents the number of postsynaptic null responses to presynaptic AP (62 $\pm$ 3 %; n=22).

The coefficient of variation is the ratio between the mean amplitude and the standard deviation of the amplitudes of the uEPSPs and represents the variability of the amplitudes of the responses (1.8 $\pm$ 0.8; n=22). This connection is characterized by a large percentage of failure of the first response which reflect a low probability of release.

Figure 3.2A shows the amplitude of the average EPSPs produced by a train of presynaptic APs at 25 Hz as a function of the stimulus number; as shown in this figure the amplitude of the postsynaptic responses increases indicating the presence of short term facilitation which is also evident in the graph of the paired pulse ratio (PPR) which

represents the ratio of the EPSP amplitudes evoked by the second and the first AP in the 25 Hz train (figure 3.2B).

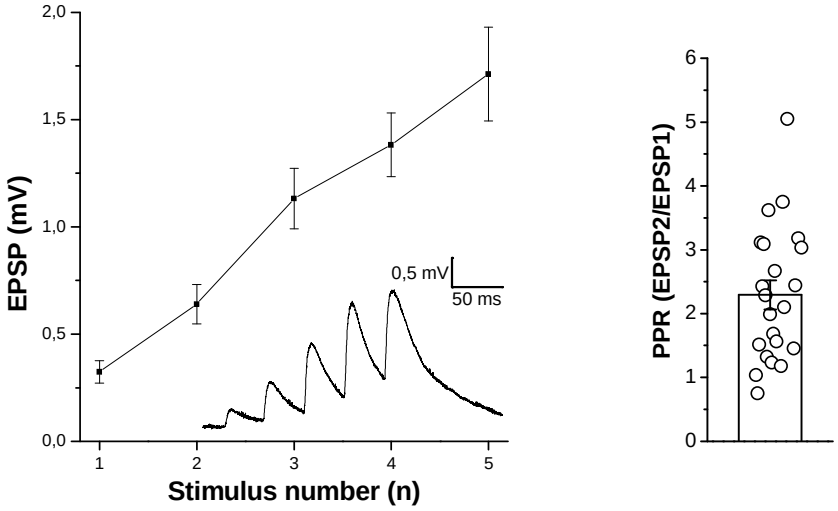

Figure 3.2. **Most excitatory connections are characterized by short term facilitation during a train of action potentials at 25 Hz (paired-pulse ratio larger than 1).**

A. Average EPSP amplitude produced by a train of presynaptic APs at 25 Hz as a function of the stimulus number from 22 experiments (average $EPSP_1$: 0.32 ± 0.05 mV, $EPSP_2$: 0.64 ± 0.09 mV, $EPSP_3$: 1.13 ± 0.14, $EPSP_4$: 1.38 ± 0.15, $EPSP_5$: 1.71 ± 0.22 mV; n=22); inset: representative mean response of one experiment to the presynaptic trains at 25 Hz. B. Histogram of the paired pulse ratio (PPR) measured in 22 experiments (average PPR2/1: 2.3 ± 0.2).

3.1.2 Involvement of calcium channels in the control of glutamate neurotransmitter release at the excitatory synapses between PYR cells and GIN interneurons

Since the voltage-gated calcium channels involved in the control of neurotransmitter release at this excitatory synapse are not known and given the important role of P/Q-type calcium channels in FHM1, I performed a pharmacological approach using saturating concentrations of specific calcium channel blockers to determine the involvement of P/Q-type calcium channels at the excitatory synapse between PYR cell and GIN interneurons.

The contribution of the P/Q-type calcium channels in the control of glutamate release was investigated applying saturating concentrations of ω-Agatoxin IVA (Aga) 400 nM in the bath solution during consecutive trials of stimulation at 25 Hz.

Figure 3.3 shows the effects of the specific P/Q-type calcium channel blocker in a representative experiment. The uEPSP amplitude elicited by the fifth AP in the train

during consecutive trials as function of time before and after Aga toxin application in the extracellular solution as indicated by the horizontal red bar. The mean response before Aga application, obtained by averaging 43 responses, and after Aga application, obtained by averaging 69 responses after 10 minutes of perfusion of saturating, concentration of Aga are summarized in the inset panel.

The histogram on the right show the average percentage of inhibition of the EPSP elicited by the first AP in the train from 5 unitary connections (percentage of Aga inhibition: 100 ± 0 %). ω-Agatoxin IVA (400 nM) completely inhibits the excitatory neurotransmission at the synapse between PYR cell and GIN interneurons

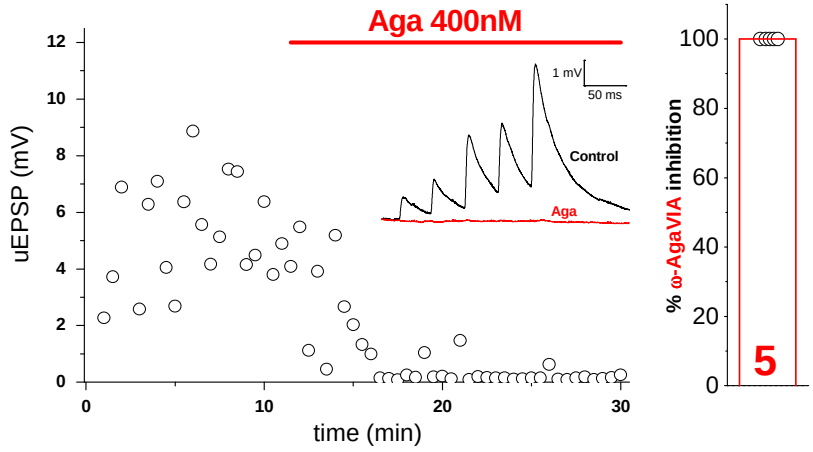

Figure 3.3. Effects of a saturating concentration of ω-Agatoxin IVA on glutamate release at the excitatory synapse between PYR cells and GIN interneurons.

On the left. uEPSPs (elicited by the fifth AP in the train) as a function of time in a representative experiment in which a saturating concentration (400 nM) of ω-Agatoxin IVA (Aga) was perfused in the extracellular solution at the time indicated by the horizontal bar (each point was obtained as average of the uEPSPs in two consecutive trials). Inset: EPSP before and after Aga obtained by averaging 43 and 69 responses. (% of inhibition of the EPSP elicited by the first AP in the train: 100 ± 0; n=5).

Given the important role of the N-type of calcium channels in controlling neurotransmitter release at some synapses (Ali and Nelson, 2006), I performed the same experiments in the presence of a saturating concentration (1 µM) of specific N-type calcium channel blocker ω-Conotoxin GVIA (GVIA) in the extracellular solution (Figure 3.4).

The specific blocker of N-type calcium channels inhibits a large fraction of synaptic transmission at this excitatory connection (percentage of inhibition of the EPSP elicited by the first AP in the train: 73 ± 5 %; n = 6).

In conclusion both P/Q- and N- type of calcium channels cooperate in controlling the neurotransmitter release at the excitatory synapse between PYR cells and GIN interneurons.

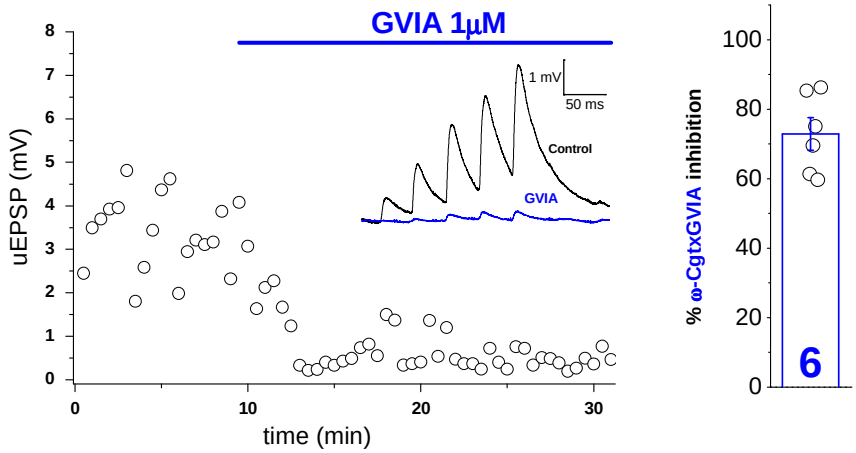

Figure 3.4. Effects of a saturating concentrations of ω-Conotoxin GVIA on glutamate release at the excitatory synapse between PYR cells and GIN interneurons.

On the left. uEPSPs (elicited by the fifth AP in the train) as a function of time in a representative experiment in which a saturating concentration of ω-Conotoxin GVIA (GVIA) 1 µM was perfused in the extracellular solution at the time indicated by the horizontal blue bar (each point was obtained as average of the uEPSPs in two consecutive trials). Inset: EPSP before and after GVIA obtained by averaging 34 and 82 responses. (% of inhibition of the EPSP elicited by the first AP in the train: 73 $\pm$ 5; n=6).

3.1.3 Characterization of inhibitory connection between GIN interneurons and PYR cells

In dual patch clamp experiments I elicited action potential (AP) in the presynaptic GIN interneuron with suprathreshold depolarizing current-injection pulses (7.5 ms duration). Once a connected pair was found, the synaptic response to a train of 5 APs at 20 Hz was recorded in the postsynaptic PYR cell hold at 0 mV in voltage clamp for at least 30 consecutive trials at 15 s intervals.

I characterized the unitary inhibitory postsynaptic currents (uIPSCs) elicited in the postsynaptic PYR cell by single APs in terms of mean amplitude (61 ± 12 pA; n=21), percentage of failures (10 ± 4 %; n=21) and coefficient of variation of the first response (0.50 ± 0.08; n=21) as shown in figure 3.5.

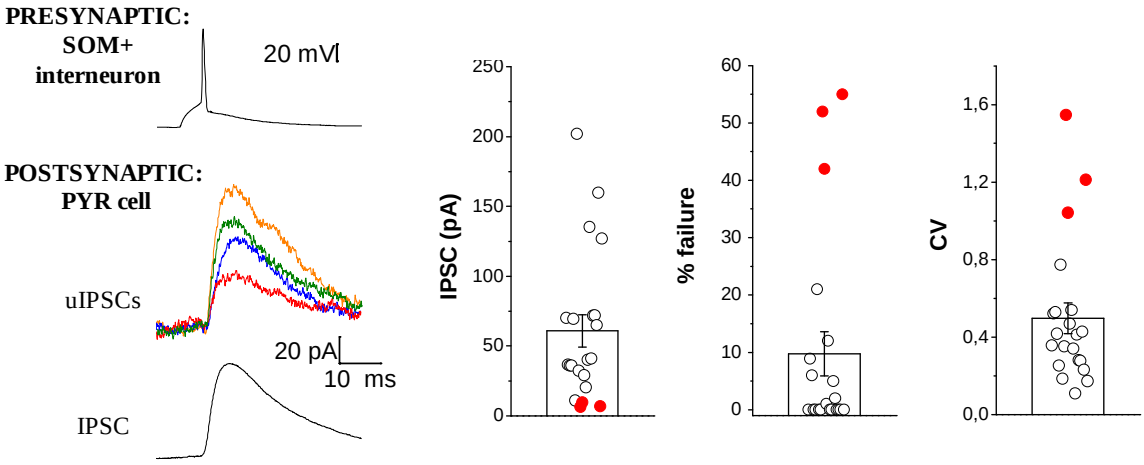

Figure 3.5. Biophysical properties of inhibitory connection between GIN interneurons and PYR cells.

On the left in the upper part: representation of the first AP of the train of five AP elicited in the presynaptic GIN interneuron; in the middle part four representative unitary IPSCs (uIPSCs) induced by first presynaptic AP of consecutive trials and down below mean uIPSC (IPSC) obtained by averaging several uIPSCs of consecutive trials including the failures.

On the right: histograms of IPSCs, percentage of failure and the coefficient of variation of the first response recorded from 21 inhibitory connections.

Red dots indicate experiments with values of % of failures and CV far away from the mean values.

Figure 3.6A shows the amplitude of the average IPSCs produced by a train of presynaptic APs at 20 Hz as a function of the stimulus number; as shown in this figure the amplitude of the postsynaptic responses decreases indicating the presence of short

term depression which is also eviden in the graph of the paired pulse ratio (PPR) which presents the ratio of the IPSC amplitudes evoked by the second and the first AP in the 20 Hz train (figure 3.6B). From the PPR histogram it's clear that most of inhibitory connections are characterized by a weak short term depression. However 3 unitary connections showed a weak short term facilitation (red dots). The same connections are also characterized by percentage of failures and CV much larger than the mean values (cfr red dots in figure 3.5)

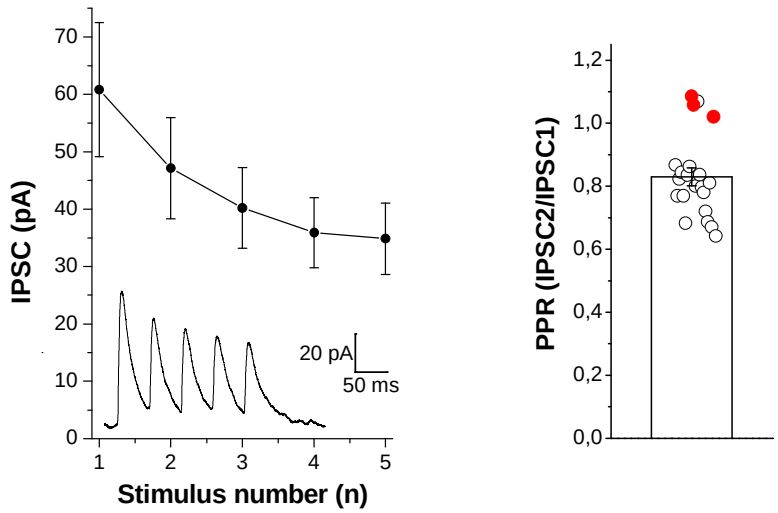

Figure 3.6 Most inhibitory connections are characterized by short term depression during a train of action potentials at 20 Hz.

A. Average IPSC amplitude produced by a train of presynaptic APs at 20 Hz as a function of the stimulus number from 21 experiments (average $IPSC_1$: 61 ± 12 pA, $IPSC_2$: 47 ± 9 pA, $IPSC_3$: 40 ± 7 pA, $IPSC_4$: 36 ± 6 pA, $IPSC_5$: 35 ± 6 pA); inset: representative mean response of one experiment to the presynaptic trains at 20 Hz. B. Histogram of the mean paired pulse ratio (PPR) obtained by averaging PPR of 21 experiments (mean PPR2/1: 0.83 ± 0.03).

Red dots indicate outliner experiments presented also in the figure 3.5.

3.1.4 Involvement of calcium channels in the control of glutamate neurotransmitter release at the inhibitory synapses between GIN interneurons and PYR cells.

I performed pharmacological experiments with specific calcium channels blockers to determine the contribution of different types of calcium channels in controlling the neurotransmitter release at the inhibitory synapses between GIN interneurons and PYR cells.

The application of a saturating concentration (400 nM) of Aga in the extracellular solution during consecutive trials of stimulation of five APs at 20 Hz shows that P/Q-type calcium channels are very important in controlling the neurotransmitter release at GIN interneurons and PYR cells synapses: in fact the average percentage of inhibition of the IPSC elicited by the first AP in the train from 5 unitary connections is 98 ± 2 % (n=5) (Figure 3.7).

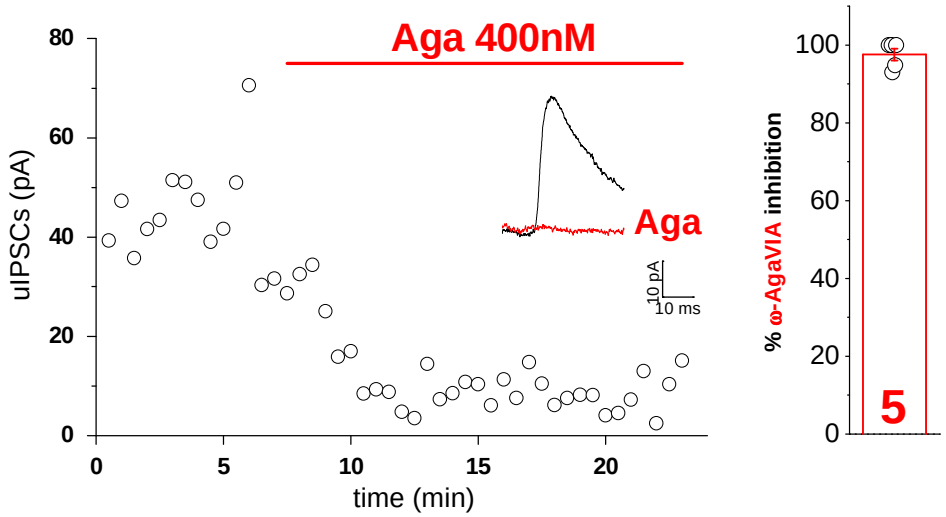

Figure 3.7. Effects of a saturating concentration of ω-Agatoxin IVA on GABA release at the inhibitory synapse between GIN interneurons and PYR cells.

Left panel: uIPSCs (elicited by the first AP in the train) as a function of time in a representative experiment in which a saturating concentration (400 nM) of ω-Agatoxin IVA (Aga) was perfused in the extracellular solution at the time indicated by the horizontal bar (each point was obtained as average of the uIPSCs in three consecutive trials). Inset: IPSC before and after Aga application obtained by averaging 43 and 50 unitary IPSCs. (% of inhibition of the IPSC elicited by the first AP in the train: 98 ± 2; n=5).

The involvement of N-type in the control of neurotransmitter release at this inhibitory synapse was studied by applying saturating (1 µM) concentrations of ω-Conotoxin GVIA (GVIA.

The application on GVIA in bath solution during consecutive trials of stimulation at 20 Hz reveals that GVIA inhibits 70 ± 3 % of the IPSC elicited by the first AP in the train (figure 3.8).

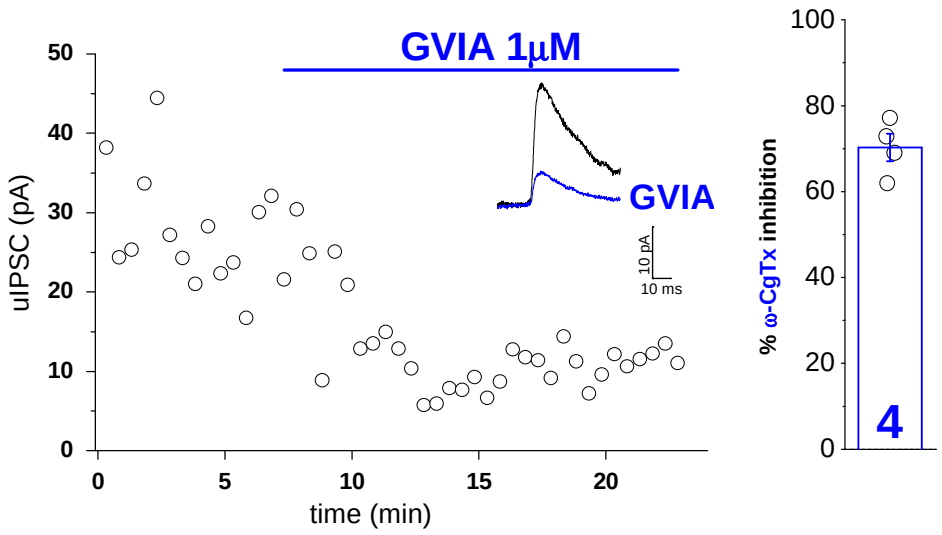

Figure 3.8. Effects of saturating concentrations of ω-Conotoxin GVIA on the GABA release at the inhibitory synapse between GIN interneurons and PYR cells.

Left panel: uIPSCs (elicited by the first AP in the train) as a function of time in a representative experiment in which a saturating concentrations (1 μM) of ω-Conotoxin GVIA (GVIA), was perfused in the extracellular solution at the time indicated by the horizontal bar (each point was obtained as average of the uIPSCs in three consecutive trials). Inset: IPSC before and after GVIA application obtained by averaging 27 and 98 unitary IPSCs.

Right histogram: percentage of inhibition of the IPSC elicited by the first AP in the train: 70 ± 3; n=4.

3.1.5 Characterization of firing properties of GIN interneurons.

To verify whether inteneurons in the outliner connection (red dots figure 3.5 and 3.6) have different firing properties I analyzed the excitability properties of interneurons of which I studied the excitatory or inhibitory connections with PYR cells. Excitability properties of GIN interneurons were studied by injecting increasing amplitude current steps in these interneurons held at -70 mV in current clamp.

Blue and green dots represent two typical firing of GIN interneurons characterized by excitability properties almost opposite between each others.

I analyzed the parameters of the first action potential induced in a GIN interneurons by 1 s pulse of suprathreshold current injection; figure 3.9A shows the resting potentials, the AP threshold, the spike width at half height and the amplitude of AHP; all these parameters analyzed show a uniform distribution of different excitability properties. Moreover GIN interneurons of outliner inhibitory connections marked by red dots are characterized by firing properties similar to other interneurons.

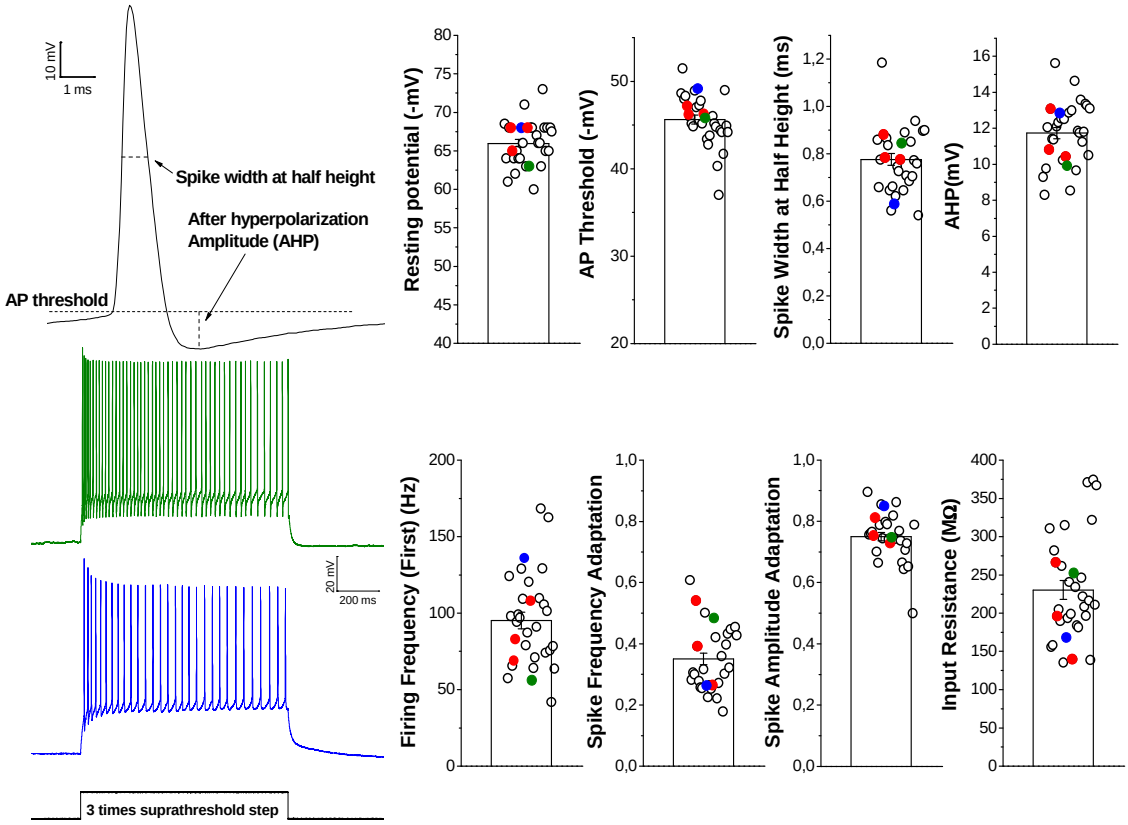

Figure 3.9. Excitability properties of GIN interneurons of connected pairs with PYR cell of layer 2/3 of somatosensory cortex.

Red dots represent outliner inhibitory connections highlighted in figures 3.5 and 3.6. Blue and green dots show the parameters of the two representative firing recorded from two different GIN interneurons represented on the left.

A. Excitability properties of the first action potential induced in GIN interneurons (in current clamp at –70 mV) by a 1 s pulse of suprathreshold current injection. Resting Potential: -66,0 ± 0,5 mV, n=31; Action Potential Threshold: -45,6 ± 0,5 mV, n=31; Spike Width at Half Height: 0,78 ± 0,02 ms, n=31; After Hyperpolarization Amplitude (AHP): 11,7 ± 0,3 mV, n=31.

B. Excitability properties of GIN interneurons (in current clamp at -70 mV) in response to a pulse of 3 times suprathreshold current injection. Firing frequency (first) was obtained as the inverse of the first interspike interval (95 ± 5 Hz, n=31). Spike frequency adaptation was obtained as the ratio between the first and last interspike interval (0,35 ± 0,02; n=31). Spike amplitude adaptation was obtained as the ratio between the last and the fist AP amplitude (0,75 ± .0,01; n=31); Input Resistance: 230 ± 12 MΩ, n=31.

Figure 3.9B show the distribution of excitability properties of GIN interneurons at high rates of current injections: in particular I analyzed firing frequency first (the reverse of the first interspike interval), the spike frequency adaptation (the ratio between the first and the last interspike interval) and spike amplitude adaptation (the ratio between the last and the first AP amplitude) and input resistance. I found that GIN interneurons

display more heterogeneity at high rates of firing parameters such as firing frequency, spike frequency and amplitude adaptation and input resistance. However GIN interneurons of outliner inhibitory connections show firing properties similar to other GIN interneurons.

In conclusion GIN interneurons in the outliner connections don’t show excitability properties different from those of most interneurons.

3.2.1 Spontaneous excitatory and inhibitory activity recorded from layer 2/3 PYR cell of primary somatosensory cortex in WT mice

We recorded spontaneous excitatory and inhibitory postsynaptic currents (sEPSCs and sIPSCs respectively) from layer 2/3 PYR cell in the presence of spontaneous ongoing network activity.

Slices were incubated in a modified ACSF (artificial cerebrospinal fluid) that more closely mimics rodent brain interstitial fluid.

To isolate the excitatory and inhibitory activity without using drugs, which would alter the network activity, we recorded the sEPSCs at reversal potential for the inhibitory input (-79 mV) and the sIPSCs at the reversal for the excitatory input (+ 10 mV) with a cesium containing intracellular solution.

Voltage clamp recordings of sEPSC from WT mice revealed two types of activity (figure 3.10): the first type of activity is characterized by spontaneous postsynaptic currents (sPSCs) which arise from uncorrelated and random spontaneous activity of presynaptic excitatory neurons which make synapses onto the patched PYR cell; the second type of activity is characterized by high amplitude large bursts of sPSCs which arise from correlated activity of a large population of presynaptic connected neurons generated perhaps through network mechanisms.

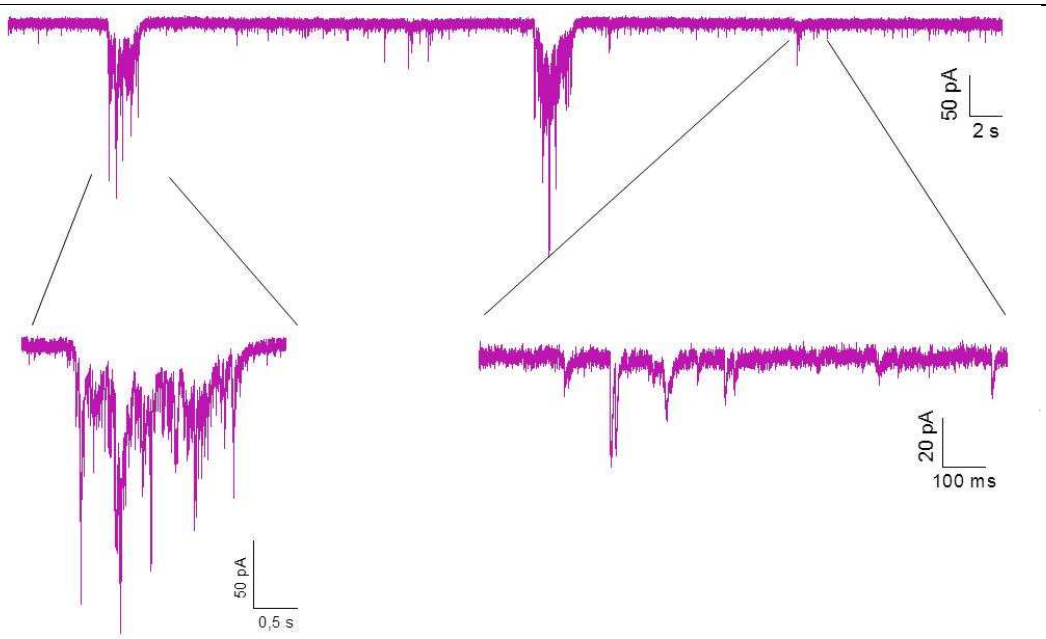

Figure 3.10. Representative recording in voltage clamp of sEPSCs from a layer 2/3 PYR cell of WT mice reveals two type of activity.

Up trace: 60 s recording of sEPSCs from a layer 2/3 PYR cell revealing two completely different types of activity expanded down below.

Down traces: representative expanded traces of the two types of activity; on the left there's 3 s of the correlated activity of large excitatory bursts with high amplitude; on the right 1.2 s of the uncorrelated activity composed by low amplitude random inputs.

Similarly recordings of sIPSCs from layer 2/3 PYR cells in voltage clamp revealed two types of activity (Figure 3.11): the first one characterized by spontaneous postsynaptic currents (sPSCs) which arise from uncorrelated and random spontaneous activity of presynaptic inhibitory interneurons which make synapses onto the recorded cell; the second one characterized by high amplitude large bursts of sPSCs which arise from correlated activity of a large population of presynaptic connected interneurons generated perhaps through network mechanisms.

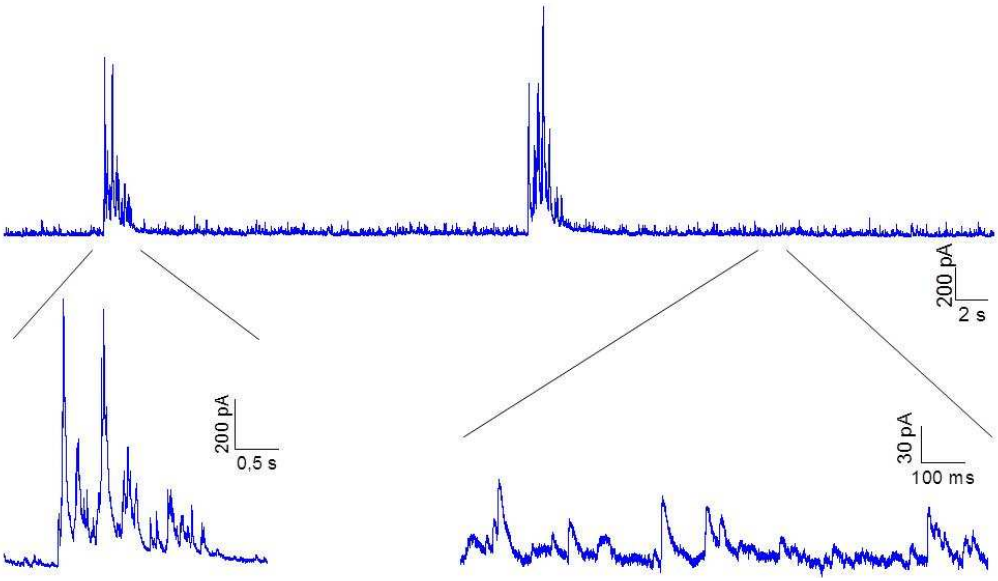

Figure 3.11. Representative recording in voltage clamp of sIPSCs from a layer 2/3 PYR cell of WT mice reveals two type of activity.

Up trace: 60 s recording of sIPSCs from a layer 2/3 PYR cell revealing two completely different types of activity expanded down below.

Bottom traces: representative expanded traces of the two types of activity; on the left there's 3 s of the correlated activity of large excitatory bursts with high amplitude; on the right 1.2 s of the uncorrelated activity composed by low amplitude random inputs.

3.2.2 Large bursts occur synchronously in nearby PYR cells and generate up states in current clamp

Dual patch-clamp recordings from 2 nearby layer 2/3 PYR cells of sEPSCs (at the reversal potential for inhibitory inputs) in one cell (cell 1 in figure 3.12) and sIPSCs (at the reversal of excitatory inputs) in the other cell (cell 2 In figure 3.12) show that the large excitatory and inhibitory bursts of correlated activity occur synchronously in the two distinct PYR cells suggesting that they are generated by network recurrent activity involving large population of connected presynaptic excitatory and inhibitory neurons (figure 3.12). In contrast, the uncorrelated sPSCs occur asynchronously suggesting that they are generated by asynchronous firing activity of connected presynaptic neurons besides AP-indipendent miniature PSC. (figure 3.12).

The large excitatory and inhibitory bursts of activity are characterized by amplitudes that are linearly correlated indicating that the larger the excitatory drive the larger is inhibitory drive.

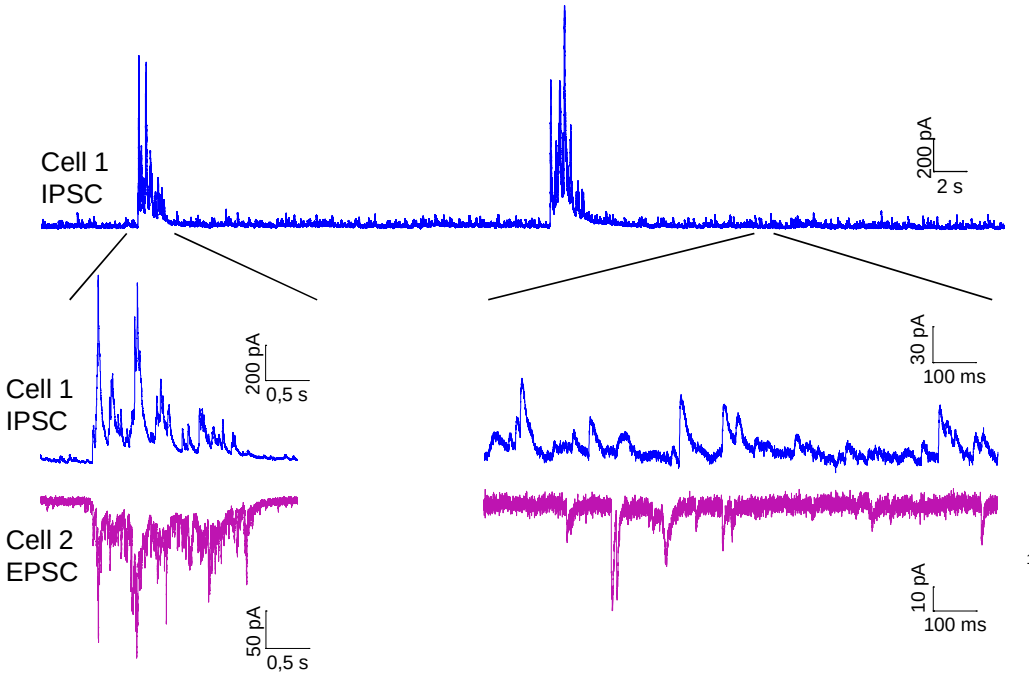

Figure 3.12. Large bursts of sEPSCs and sIPSCs occur synchronously during ongoing network activity whereas uncorrelated excitatory and inhibitory activities are not synchronous.

Up trace. 60 s recording of sIPSCs from a layer 2/3 PYR cell revealing two completely different types of activity expanded down below.

Bottom traces: on the left expanded 3 s of correlated activity of large inhibitory burst recorded from the first PYR cell that occurs synchronously with the large excitatory burst recorded from a second nearby PYR cell; on the right 1.2 s of uncorrelated inhibitory activity which occurs asynchronously with the uncorrelated activity recorded by the second nearby PYR cell.

This reflects the architecture of local cortical circuits, in which PYR cells are connected to other PYR cells (positive feedback loops) and to inhibitory interneurons (negative ffeback loops) in a way that dynamically maintains the excitation-inhibition balance during cortical network activity.

Dual patch-clamp recordings in current clamp in one PYR cell (cell l in figure 3.13) and in voltage clamp in the other (cell 2 in figure 3.13) reveal that large amplitude membrane potential fluctuations associated with spiking activity (resembling the "up states" recorded *in vivo* during anesthesia and quiet wakefulness; Steriade et al.,1993) occur synchronously with the large bursts of sPSCs (figure 3.13). The up states are driven by the large barrages of synaptic potentials generated through the recurrent network mechanisms that underlie the large sPSCs bursts.

Spontaneous firing activity is not present during down states indicating that layer 2/3 PYR cells do not show non-synaptically driven intrinsic firing and that the uncorrelated synaptic activity is not sufficient to elicit APs in these cells.

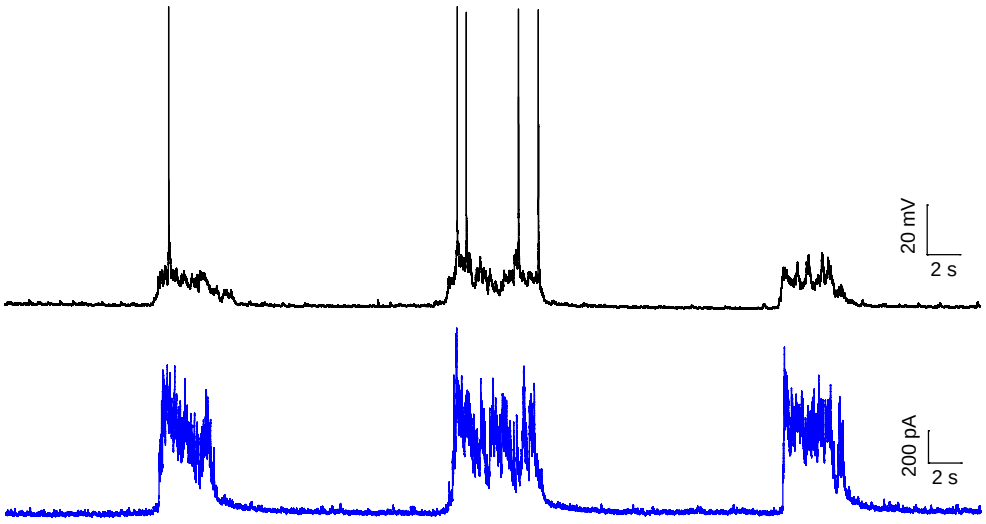

Figure 3.13. Bursts recorded in voltage clamp from 1 PYR cell are correlated with the up-states recorded in current clamp from another nearby PYR cell.
Upper trace: current clamp 60 s recording from one PYR cell hold at resting potential.
Down trace: 60 s of voltage clamp recording from a nearby PYR cell in which sIPSCs have been recorded. Large bursts of PSCs (inhibitory and excitatory) underlie the UPS recorded in current clamp. Spike activity recorded in current clamp is present only during UPS.

On the basis of dual patch clamp recordings Alessandra Fabbro established some threshold values of amplitude and duration to distinguish the correlated synchronous activity of large bursts from the uncorrelated asynchronous PSCs to analyze these two different types of activity in separate way.

3.2.3Excitatory and inhibitory uncorrelated asynchronous sPSCs in PYR cells of WT and R192Q FHM1 KI mice.

As mentioned the uncorrelated sEPSCs include miniature EPSCs (mEPSCs) due to stochastic neurotransmitter glutamate release and AP-driven excitatory inputs due to spontaneous asynchronous firing of connected excitatory (mainly PYR) neurons.
We obtained the total uncorrelated excitatory synaptic charge by integrating the uncorrelated sEPSCs over the total recording time in slices of WT and R192Q KI mice.

We found that the total excitatory synaptic charge of uncorrelated asynchronous sEPSCs is larger in R192Q KI mice compared to WT mice (figure 3.15A). Previous studies on mEPSC showed that frequency and amplitude of mEPSCs were not altered in R192Q KI mice (Tottene et al., 2009) indicating the absence of homeostatic compensatory mechanisms (Turrigiano and Nelson, 2004). Additionally the synaptic charge of the mEPSC which represent a large fraction of the asynchronous excitatory synaptic charge (dotted line in figure 3.14A) was unaltered.

These findings suggest that the increase in uncorrelated asynchronous charge of sEPSCs is due to an increase in the AP-drive excitatory inputs.

The increase in the asynchronous excitatory synaptic charge onto PYR cells found in R192Q KI mice is consistent with the enhanced glutamate release, and increased excitatory synaptic transmission found at PYR cells synapses of KI mice (Tottene et al, 2009).

The uncorrelated inhibitory PSCs include miniature IPSCs (mIPSCs) due to stochastic AP-independent GABA release and AP-driven inhibitory inputs due to spontaneous asynchronous firing of different types of neighboring connected interneurons. We obtained the total uncorrelated inhibitory synaptic charge by integrating over the total recording time the uncorrelated sIPSCs in slices of WT and R192Q KI mice.

We found that the inhibitory synaptic charge of uncorrelated sPSCs is not altered in KI mice

mIPSCs were recorded by applying TTX (0.2 µM), APV (50 µM) and NBQX (2 µM) in the bath solution to block voltage-dependent Na^+ channels, AMPA, NMDA and kainate glutamate receptors. I found that mIPSC frequency and amplitude are unaltered in R192Q KI mice suggesting the absence of homeostatic compensatory mechanisms (mIPSC amplitude WT: 21.1 $\pm$ 1.4 pA, n = 6 vs KI: 20.4 $\pm$ 1.5 pA, n=6; p = 0.75. mIPSC frequency WT: 7.4 $\pm$ 1.5 Hz, n = 6 vs KI 5.5 $\pm$ 0.5 Hz, n=6; p = 0.24). The miniature inhibitory synaptic charge represents about 50 % of the total asynchronous inhibitory charge as represented by dotted line in figure 3.14B and are similar in WT and KI mice.

The unaltered uncorrelated inhibitory synaptic drive onto KI PYR cells is consistent with unaltered inhibitory transmission at synapses of FS and other types of intemeurons contributing to the sIPSCs (including the intemeurons that show spontaneous intrinsic firing, that are not FS intemeurons because these intemeurons do not show spontaneous intrinsic firing in our experimental conditions).

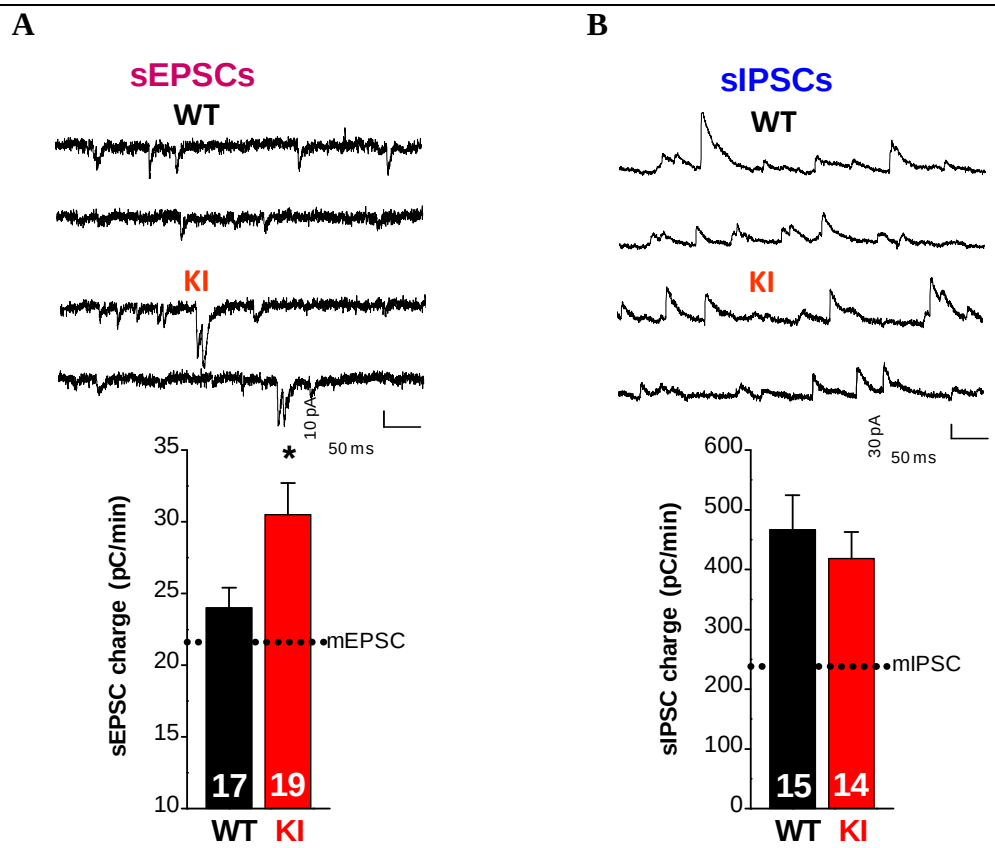

Figure 3.14. The synaptic charge of uncorrelated asynchronous sEPSCs is increased in R192Q KI mice whereas the synaptic charge of uncorrelated asynchronous sIPSCs is unaltered.

A. Representative uncorrelated asynchronous sEPSCs recordings (1s) from WT and KI mice. The histogram represents sEPSC synaptic charge calculated as the integral over the total recording time of uncorrelated asynchronous activity (mean excitatory synaptic charge WT: 24 ± 1 pC/min, n=17 and KI 31 ± 2 pC/min, n=19); mEPSCs and mIPSCs synaptic charge were calculated as the integral over the recording time of mEPSCs and mIPSCs from WT and KI mice in presence of specific toxins in bath solutions. Since miniature synaptic charges were similar between WT and KI mice, we pulled together those values to obtain an averaged excitatory and inhibitory miniature synaptic charge (mean synaptic charge of mEPSCs: 21.6 ± 1.7 pC/min; n=8; mean synaptic charge of mIPSCs: 238 ± 19 pC/min; n=12**)**

3.2.4Spontaneous synchronous bursts of sPSCs in layer 2/3 PYR cells of WT and R192Q FHM1 KI mice

We calculated the integrals of all the bursts over the total recording time to measure the total excitatory and inhibitory burst charge onto the same layer 2/3 pyramidal cell.

We found that both the total excitatory burst charge and the total inhibitory burst charge are increased in R192Q KI mice (figure 3.15A). The ratio between excitatory and

inhibitory synchronous charges, obtained from the mean of the ratio between the total excitatory and inhibitory burst charge of every experiment, results unaltered in R192Q KI mice (figure 3.15B). This findings suggest that FHM1 mutations don't alter the excitation-inhibition balance during spontaneous network activity.

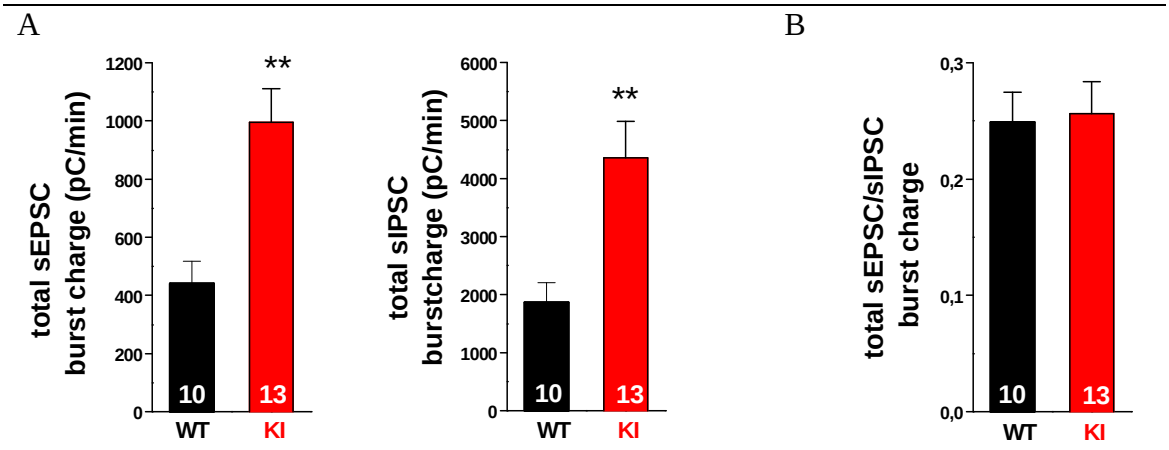

Figure 3.15. Total excitatory and inhibitory burst charges are increased in R192Q KI mice whereas their ratio is unaltered in KI mice.

A. total excitatory and inhibitory burst charge, calculated as integrals of all the excitatory bursts over the total recording time, is increased in R192Q KI mice (sEPSCs bursts: WT 0.44 $\pm$ 0.77 nC/min, n=10; KI 1.00 $\pm$ 0.12 nC/min, n=13, $p < 0.01$; sIPSCs bursts: WT 1.86 $\pm$ 0.34 nC/min, n=10; KI 4.35 $\pm$ 0.63 nC/min; n=13, $p < 0.01$).

B. The ratio of total synchronous excitatory and inhibitory synaptic charge is unaltered in R192Q KI mice (total sESPC/sIPSC burst charge: WT 0.25 $\pm$ 0.03, n=10; KI 0.26 $\pm$ 0.03).

The maintenance of excitation-inhibition balance during synchronous correlated activity is confirmed by the analysis of the mean instantaneous synaptic charge calculated as the integral of each burst over its duration; in fact both the instantaneous excitatory synaptic charge (WT 76 $\pm$ 10 pC/s, n=10; KI 79 $\pm$ 7 pC/s, n=13; figure 3.17A) and the instantaneous inhibitory synaptic charge (WT 308 $\pm$ 43 pC/s, n=10; 336 $\pm$ 38 pC/s, n=13; figure 3.17A) are similar in WT and R192Q KI mice. Indeed the ratios between instantaneous excitatory and inhibitory synaptic charges (figure 3.17C) are similar in WT and KI mice but also similar to the ratio between the total excitatory and inhibitory burst charge. These results suggest that the increase in the total excitatory and inhibitory synaptic charge bursts in R192Q KI mice is not due to an increase in the instantaneous burst charge.

The analysis of burst frequency and duration shows that the increase is due mainly to higher frequency of the synchronous bursts in R192Q KI than in WT mice (figure

3.17A) whereas it's not clear if bursts duration are increased in R192Q KI mice (burst EPSC duration: WT 5.1 ± 0.4, n=10; KI 5.8 ± 0.4, n=10; p >0.05. Burst IPSC duration: WT 5.2 ± 0.4, n=10; KI 6.3 ± 0.4, n=13; p<0.05).

The increase in frequency of excitatory and inhibitory bursts confirm previous data obtained in this laboratory studying the frequencies of up states in WT and R192Q KI mice (UPS frequency WT 1.55 ± 0.11, n=21 ; KI 1.99 ± 0.13, n=26; p <0.05; Fabbro et al., unpublished data).

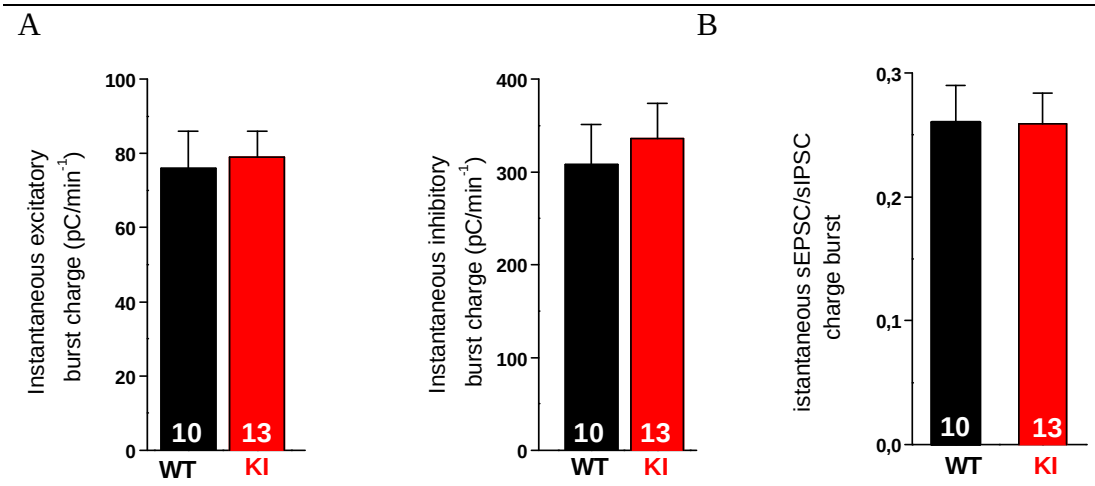

Figure 3.17. Istantaneous excitatory and inhibitory burst charges are similar in WT and in KI mice

A. Mean instantaneous excitatory and inhibitory burst charge obtained averaging the mean ratios between the integral of each burst and its duration (instantaneous excitatory burst charge WT 76 ± 10 pC/s, n=10; KI 79 ± 7 pC/s, n=13; instantaneous inhibitory burst charge WT 308 ± 43 pC/s, n=10; 336 ± 38 pC/s, n=13).

B Istantaneous excitatory inhibitory charge burst ratio obtained averaging the mean ratios from severale experiments (WT 0.26 ± 0.03, n=10; KI 0.26 ± 0.03, n=13).

The increase of burst frequencies in R192Q KI mice leads to an important functional consequence of R192Q mutation: there's an increase in the fraction of time spent by the cortical network in the spontaneous synchronous activity calculated as the sum of burst durations over the total recording time (time of excitatory synchronous network activity WT 9.6 ± 0.9 %, n=10; KI 20.6 ± 1.2 %, n=13; p< 0.001. tine of inhibitory synchronous network activity WT 10.6 ± 1.2 %, n=10; KI 21.2 ± 1.3, n=13; p < 0.001. figure 3.18B).

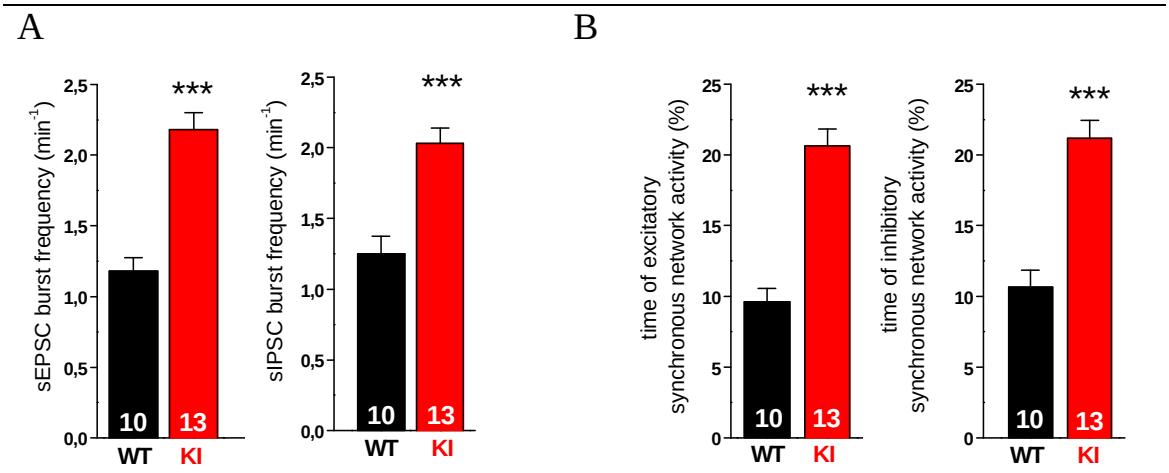

Figure 3.18 the increase in the total excitatory and inhibitory burst charge in R192Q KI mice is due to an increase in frequency of synchronous bursts which leads an increase in the fraction of time spent in synchronous activity by the cortical network.

A. histograms of excitatory (on the left) and inhibitory (on the right) burst frequency showing an increase of frequency in KI mice (excitatory burst frequency WT 1.18 $\pm$ 0.09; n=10; KI 2.18 $\pm$ 0.12, $p < 0.001$; inhibitory burst frequency 1.25 $\pm$ 0.12, n=10; KI 2.03 $\pm$ 0.11, n=13, $p < 0.001$).

B. Histograms of percentage of time spent in synchrounous excitatory (on the left) and inhibitory (on the right) network activity showing an increase in KI mice (time of excitatory synchronous network activity WT 9.6 $\pm$ 0.9 %, n=10; KI 20.6 $\pm$ 1.2 %, n=13; $p < 0.001$. tine of inhibitory synchronous network activity WT 10.6 $\pm$ 1.2 %, n=10; KI 21.2 $\pm$ 1.3, n=13; $p < 0.001$)

4. DISCUSSION

4.1 Study of excitatory and inhibitory synaptic transmission between pyramidal cell and fluorescent somatostatin-expressing interneurons

The first aim of this thesis was to characterize synaptic transmission between PYR and another type of inhibitory internerneuron, somatostatin (SOM)-expression interneurons (Martinotti cells, MC), and to establish whether P/Q-type Ca2+ channels are involved in controlling neurotransmitter release at the excitatory PRY-SOM synapse and inhibitory SOM-PYR synapse.

We took advantage of a particular strain of transgenic mice (GFP-expressing interneurons, GIN) which expresses EGFP in a subpopulation of somatostatin-positive (SOM^+) interneurons (GIN interneurons).

The excitatory synaptic connections between PYR cell and GIN interneurons are characterized by a strong facilitation that grows non-linearly in response to 5 presynaptic APs at 25 Hz (paired pulse ratio, PPR2/1: 2.3 $\pm$ 0.2; n=22; the response elicited by the fifth presynaptic AP is five times larger compared to that elicited by the first AP). This indicates that interneurons can be efficiently recruited by PYR cells during high-frequency network activity.

The inhibitory connection between GIN inteneurons and PYR cells is characterized by a relatively weak short-term depression in response to 5 presynaptic APs at 20 Hz stimuli (PPR2/1: 0.83 $\pm$ 0.3; n=21; the response elicited by the fifth presynaptic AP is decreased by about 40% compared to that elicited by the first AP). Tottene et al., (2009) showed that at the inhibitory synapse between FS and PYR the response to the fifth presynaptic AP is decreased by about 60% compared to the first response. This suggests that during sustained activity GIN interneurons can inhibit PYR cells for a longer period than FS interneurons.

The data on short term depression and facilitation suggest that SOM^+ interneurons could be particularly important to prevent over-excitation during sustained cortical activity.

In addition to this weakly depressing inhibitory synapses I also found that there is a minority of inhibitory synaptic connections that exhibit a weak synaptic facilitation. This could be due to the heterogeneity that characterize the SOM+ inteneurons.

Several groups have demonstrated that the fluorescent interneurons SOM+ can be divided in different groups according to firing and morphological properties (Halabinsky et al., 2006; McGarry et al., 2010).

The heterogeneity in the interneurons expressing GFP reflect that GIN mice have been created by pronuclear microinjection of trangene DNA which is integrated randomly in the mouse genome.

Nevertheless all the SOM+ interneurons studied in this thesis had very similar intrinsinc excitability properties and this is shown by analysis of firing properties of all fluorescent SOM+ interneurons recorded (n=54, not shown). We cannot exclude that other properties of SOM+ interneurons, not investigated in this thesis, may account for the heterogeneity found in the inhibitory connections.

I used a pharmacological approach to determine the contributions of Ca^{2+} channels at both excitatrory and inhibitory synapse between PYR cell and GIN interneurons. By evaluating the fraction of inhibition of the synaptic responses by ω-agatoxin IVA (specific pharmacological blockers of P/Q-type Ca^{2+} channel), I showed that P/Q-type Ca^{2+} channel play a predominant role in controlling the release of glutamate and GABA at both excitatory PYR-SOM and inhibitory SOM-PYR synapses. Interestingly blocking N-type Ca^{2+} channels with ω-conotoxin GVIA also inhibited a large fraction of post-synaptic potentials or currents at both excitatory and inhibitory synapses between GIN interneurons and PYR cells. These results indicate a superadditivity on EPSP and IPSC inhibition by ω-agatoxin IVA and ω-conotoxin GVIA. Small changes in amplitude or time course of the local concentration of intracellular Ca^{2+} within the synaptic terminals are very effective in modulating the amount of transmitter released. Considering the nonlinear power relationship between presynaptic Ca^{2+} influx and neurotransmitter release (Scheneggenburger and Neher, 2000) the superadditivity of fractional EPSP or IPSC inhibition by the two toxins indicates that P/Q and N-type Ca2+ channels cooperate in controlling the neurotransmitter release at both excitatory and inhibitory synapses between PYR cells and SOM^{+} interneurons.

Given the predominant role of P/Q-type Ca^{2+} channels in controlling the neurotransmitter release at both excitatory and inhibitory synapses, it will be interesting to study excitatory and inhibitory neurotransmission in GIN mice carrying R192Q FHM1 mutation. Tottene et al., (2009) previously showed that the gain of function of glutamate release found at PYR-FS synapses in R192Q KI mice is due to an increase of probability release at these synapses. A similar gain of function could be hypothesized at the PYR-SOM+ synapses. An increase in the release probability could reduce short term facilitation or even reverse it to depression thereby altering the whole network activity.

Regarding the inhibitory connection between SOM+ and PYR cells, if the unaltered inhibitory neurotransmission at FS-PYR synapses previously observed by Tottene et al. (2009) is a general feature of cortical inhibitory synapses, an unaltered inhibitory neurotransmission could also be expected also at SOM^{+}-PYR synapses. These hypothesis is partially confirmed by the analysis of spontaneous synaptic activity presented in this thesis (see next paragraph).

4.2 Study of the total amount of excitatory and inhibitory synaptic charge onto a pyramidal cell

To test the general hypothesis that FHM1 mutations might lead to an unbalance between inhibition and excitation towards excitation I investigated the excitatory and inhibitory amount of charge received by a layer 2/3 PYR cell during ongoing network activity without any type of stimulation. Voltage clamp recordings of spontaneous excitatory and inhibitory activity showed the presence of two types of activities.

1) The first one is represented by uncorrelated inputs that occur asynchronously in two pyramidal neurons recorded simultaneously. This uncorrelated spontaneous post synaptic currents (sPSCs) are due to uncorrelated firing activity of connected presynaptic (excitatory and inhibitory) neurons, and to AP-independent mimiature post synaptic currents (mPSCs) which are due to stochastic neurotransmitter release at synaptic terminals.

I found an increase in uncorrelated excitatory synaptic charge in R192Q KI compared to WT mice. This increase reflects an increase in the synaptic charge due to spontaneous spiking output of connected excitatory (mainly pyramidal) neurons, as mEPSC synaptic charge was similar between WT an KI mice. The increased uncorrelated excitatory synaptic drive onto KI pyramidal cells is consistent with increased excitatory synaptic transmission at recurrent PYR cell synapses and confirms and extends the finding of enhanced evoked glutamate release at PYR cell synapses of KI mice (Tottene el., 2009). By contrast, the total uncorrelated inhibitory synaptic charge onto individual PYR cells was similar between KI and WT mice. About 50% of this uncorrelated inhibitory synaptic charge is due to spontaneous spiking output of connected inhibitory interneurons (mIPSCs). The unaltered uncorrelated inhibitory synaptic drive onto KI PYR cells is consistent with unaltered inhibitory transmission at synapses of FS and other types of intemeurons contributing to the sIPSCs. Despite the relative unbalance

towards excitation in the R192Q KI mice, the uncorrelated synaptic inputs remain below firing threshold at resting potential during down states in layer 2/3 PYR cells in both WT and KI mice.

2) The second type of activity is generated by correlated activity of a large population of connected presynaptic (excitatory and inhibitory) neurons through recurrent network mechanisms. We have shown that these large bursts elicited by the spontaneous synchronous network activity underlie the fluctuations of membrane potential in current clamp similar to the up states recorded *in viv*o and *in vitro* (Sanchez-Vives and McCormick, 2000; Steriade et al., 1993).

I also showed an increase in the total correlated excitatory and inhibitory synaptic charge (generated through recurrent network mechanisms) in Rl92Q KÌ compared to WT mice. The ratio of the total synchronous excitatory and inhibitory synaptic charges on individual PYR cells is unaltered in the R192Q KI mice. A similar value is obtained for the ratio of the instantaneous excitatory and inhibitory synaptic charges within the individual PSC bursts. The instantaneous excitatory synaptic charge and the instantaneous inhibitory synaptic charge during these bursts were both similar in WT and KI mice. These findings indicate that during the spontaneous network activity the excitation-inhibition balance is not altered in R192Q KI mice.

The increase in the total excitatory and inhibitory synaptic charges is mainly caused by increase in frequency of the synchronous bursts in KI mice. This change in burst frequency leads to an increase of the fraction of time spent by the cortical network in spontaneous synchronous activity. This important functional consequence of the FHMl mutation is supported by current clamp recordings performed in our laboratory which have shown an increase in the fraction of time spent by PYR cells in up states as a consequence of both an increased frequency and duration of the up states.

It remains to be established whether the unbalance of the uncorrelated synaptic inputs onto pyramidal cells towards excitation and the increase in the fraction of time spent by the cortical network in spontaneous synchronous activity in Rl92Q KI mice are correlated and causally linked.

In conclusion, FHM1 mutations do not alter the excitation-inhibition balance during the spontaneous synchronous network activity that generates the up states and, as a consequence, they produce relatively small alterations of the spontaneous synaptically driven spiking activity of cortical PYR cells.

These data suggest that in normal conditions the differential effects of FHM1 mutations on excitatory and inhibitory neurotransmission may leave excitation-inhibition balance

within a range of physiological limits. It would be interesting to study whether the excitation-inhibition balance can be disrupted during activity evoked by prolonged repetitive thalamic and/or local extracellular stimulation (that might mimic the condition of intense, long-lasting sensory stimulation, which is one of the known migraine triggers).

5. MATERIALS AND METHODS

5.1 Experimental procedures for the study of spontaneous activity

5.1.1 Animals

The study of spontaneous activity was performed using WT C57Bl/6J mice (genetic background: 87.5 %) and the corresponding KI strains carrying the $Ca_V2.1$ R192Q FHM1 mutation in omozygosis as described in van den Maagdenberg et al. (2004).

These strains are distributed by The Jackson laboratories.

Experiments were made from postnatal day 16 to 18.

All experimental procedures were carried out in accordance with the Italian Animal Welfare Act and approved by the local authority veterinary service.

5.1.2 Coronal slices solutions

Standard Artificial Cerebrospinal Fluid (sACSF): $MgCl_2$ 1 mM, $CaCl_2$ 2 mM, NaCl 125 mM, KCl 2.5 mM, $NaHCO_3$ 25 mM, NaH_2PO_4 1,25 mM, glucose 25 mM, minocycline 50 nM saturated with 95% O_2 and 5% CO_2 (pH:7.4).

Gluconate Cutting Solution (GCS): K gluconate 130 mM, KCl 15 mM, EGTA 0,2 mM, HEPES 20 mM, glucose 25 mM, kynurenic acid 2 mM, minocycline 50 nM saturated with 100% O_2 (pH:7.4).

Mannitol Cutting Solution (MCS): D-mannitol 225 mM, glucose 25 mM, KCl 2.,5 mM, NaH_2PO_4 1.25 mM, $NaHCO_3$ 26 mM, $CaCl_2$ 0,8 mM, $MgCl_2$ 8 mM, kynurenic acid 2 mM, minocycline 50 nM saturated with 95% O_2 and 5% CO_2 (pH:7.4).

GCS, MCS e sACSF contain minocycline (SIGMA M9511), a micro-glia inhibitor, to prevent immunitari responses. GCS and MCS contain kynurenic acid (Tocris 0223), a NMDA receptor blocker.

5.1.3 Slices preparation

The slicing protocol has been developed by Dr Stephane Dieudonné (*École Normale de Paris*) working in Prof Philippe Ascher's group. This protocol is characterized by the presence of the GCS (described in Dugué et al., 2005) which mimics neuronal

intracellular ionic composition to enhance the recovery of neurons. The concentration of extracellular calcium is set to 0 mM to prevent neuronal activity.
Animals were anestethized with isofluoran and decapitated. The brain was quickly removed and put in the ice-cold sACSF. A cut perpendicular to the anteroposterior axis was made to remove the cerebellum and to create a plane surface for the coronal slice preparations.
Cutting was made on the coronal plane in ice-cold GCS with a vibratome (Leica VT1000S). Acute coronal slices containing the barrel cortex (350 µm thick) were then transferred at room temperature for 1 minute in MCS (characterized by a ionic composition intermediate between GCS and sACSF). Slices were then transferred in sACSF at 30 °C for 30 minutes and finally at room temperature for another 30 minutes to allow neurons recovering from the cutting procedure. Each slice was then maintained for at least 20 minutes in the recording solution before being used for electrophysiological recordings

5.1.4 Microscope

Slices observations and recordings were made with an upright microscope (Nikon Instruments, Eclipse E600FN) under infrared differential interference contrast (IR DIC).
Slices were first visually inspected with a 10X objective and then with a water immersion objective (60X) for a detailed observation of cells and for the electrophisiological recordings.
Two CCD cameras (Hamamatsu Photonics K.K., Hitachi) were connected to the microscope for a live view acquisition on two different displays.
Blue light was used to see fluorescent neurons in slices.
The microscope was equipped with a fluorescence lamp and a FITC filters combination that allowed to detect epi-fluorescence signals from EGFP-expressing interneurons in GIN (GFP-expressing interneurons) mice slices.

5.1.5 Patch clamp technique

The patch clamp technique allows single channel or whole cell currents to be recorded with the advantage of controlling the intracellular medium. A glass micropipette with an open tip diameter (~1-2 µm) is filled with a solution that is usually matching the ionic composition cytoplasm. A silver chloride wire is in contact with this solution and conducts electrical currents to the patch clamp amplifier. A high resistance seal between the pipette and the cell membrane (giga-ohm) is formed by pressing the pipette against the membrane (figure 2.14A) and by applying a light suction through a suction tube connected to the pipette holder (figure 2.8). The high resistance of this seal makes it

possible to record currents with high resolution and low noise. Once the giga–ohm seal is established (figure 2.14B left), the positive pressure previously applied to the pipette is released. The whole cell configuration was then achieved by applying further suction to trigger the rupture of the membrane patch (figure 2.14B right). In the whole cell configuration, the membrane is ruptured and the tip of the pipette is sufficiently wide (around 1 µm diameter) to allow the washout of the cytoplasm with a time constant described in section 2.2.8). After this time, the intracellular fluid can be considered equal to that of the intracellular medium contained in the pipette.

The patch-clamp technique offers the possibility to perform experiments in two different configurations: the voltage-clamp and the current-clamp.

The voltage clamp method

The voltage clamp method (or voltage clamp recording mode) allowed recording of ionic currents across the cell membrane at a fixed voltage and was used to record post synaptic currents in response to stimulations. In voltage clamp mode, the electrode is held at a certain command potential while measuring currents flowing down the electrode. This is achieved by a current-voltage converter that produces a voltage output that is proportional to the current input.

The current clamp method

The current clamp method (or current clamp recording mode) allowed recording the membrane potential by injecting current into a cell through the recording electrode. Unlike the voltage clamp mode where the membrane potential is held at a voltage determined by the experimenter, in the current clamp mode, the membrane potential is free to vary and the amplifier records spontaneous voltage variations or voltage deflections evoked by stimulations. Similarly to the voltage clamp recording mode, the current flow through the electrode produces a voltage drop across the electrode that depends on the product of the current and of the resistance of the electrode and this voltage drop will add to the recorded potential. In current clamp mode, the bridge balance control is used to balance out this voltage drop so that only the membrane potential is recorded.

5.1.6 Patch clamp set up and recordings

During the experiments, the slices were put in a chamber and continuously perfused with fresh extracellular solution saturated with 95% O2 and 5% CO2 at 3 ml/min.

Extracellular solution, modified Artificial Cerebrospinal Fluid (mACSF): NaCl 125 mM, KCl 3,5 mM, $NaHCO_3$ 25 mM, NaH_2PO_4 1,25 mM, $MgCl_2$ 0,5 mM, $CaCl_2$ 1 mM, glucosio 25 mM. saturated with 95% O_2 e 5% CO_2 (pH a 7.4).

Intracellular solution: KCl 6 mM, Cs metansulfonate 114 mM, HEPES 10 mM, Na phosphocreatine 10 mM, MgATP 4 mM, NaGTP 0,3 mM, biocytin 0,1 % (pH 7.25 with CsOH, osmolarity 300 mOsm).

The extracellular solution (mACSF) differs from the sACSF solution because of a concentration of K^+ ions slightly higher and a lower concentration of Ca^{2+} and Mg^{2+} ions which make mACSF more similar to the cerebrospinal fluid than sACSF solution (Chutkow et al., 1974, Zhang et al., 1990). Under these conditions the spontaneous activity of cortical circuitry is increased compared to that observed in the presence of standard solution (Sanchez-Vives et al., 2000).

Electrical signals were recorded through a Multiclamp 700B patch-clamp amplifier and digitized using a Digidata 1322A interface and pClamp software (all from Axon Instruments). Signals were low-pass filtered at 2 kHz and sampled at 10 kHz. Experiments were performed at room temperature (RT).

The pipettes for patch-clamp were obtained from borosilicate capillaries (Wiretrol II 5-000-2050) using the puller P-95 (Sutter Instruments). The resistance of pipettes in the bath ranged between 3 and 5 MΩ.

Liquid junction potential (LJP) measured at the pipette tip was -9 mV (calculated: -10 mV). LJP should be added to all voltages to obtain the correct values of membrane potential in whole-cell recordings.

Recordings of spontaneous activity were performed on layer 2/3 pyramidal (PYR) cell of somatosensory cortex (barrel cortex) from 350 µm acute coronal slices. The cells recorded were deeper than 45 µm from the surface with a dendritic arvìborization almost parallel to the plane of the cut.

PYR neurons were visually identified by triangular soma with two basal dendrites, an apical dendrite which elongates to the layer 1 and the axon spreading in the deeper layers or other cortical regions and voltage-clamped at the Cl^- reversal potential (-79 mV) for excitatory postsynaptic currents (EPSCs) recordings and at the reversal potential for excitatory currents (+10 mV) for inhibitory postsynaptic currents (IPSCs) recordings, with no series resistance (Rs) compensation (voltage values not corrected for LJP; Rs was below 28 MΩ with less than 25% variation).

For dual, simultaneous patch-clamp experiments (cells 50-140 µm apart), the internal solution used for the cell from which IPSCs were recorded was the same as described above; the one used for EPSC recordings differed in that 114 mM Cs-methanesulfonate was substituted by 114 mM K-gluconate. Spontaneous EPSCs and IPSCs were recorded for 3-8 minutes (LJP: -12 mV)

Miniature inhibitory post synaptic current mIPSCs were recorded at the reversal for excitatory inputs (sampling 10 kHz; filter 2 kHz) after spontaneous activity recording on acute coronal slices perfused with a mACSF containing TTX (0.2 µM), D-AP5 (50 µM), and NBQX (2 µM) (Tocris). Miniature IPSCs recordings started after 10 minutes of perfusion of mACSF with toxins.

5.1.7 Data analysis

Analysis was performed using the Clampfit 9.0 software of the pClamp suite (Axon Instruments). Synaptic charges were calculated from the baseline-adjusted voltage clamp recordings by integrating the current over time. EPSC and IPSC bursts durations were estimated by calculating the time between their onset (at the beginning of the inputs temporal summation over baseline) and the change of slope during the return of the current to the baseline level.
Clampfit 9.0 was used to study mIPSC; this software detects events on the basis of closeness of fit to a sliding template created (for each cell) by averaging 15–20 of its most unambiguous mIPSCs selected by eye. Each event was further visually inspected to exclude artefacts. Overlapping events were excluded from amplitude analysis.
All averages were calculated with Microsoft Excel. Graphs and statistical comparison were obtained with the Origin software (Microcal Software, Inc.). Data are given as mean ± SEM; stars indicate a statistically significant difference from control assessed by the Student's t test (*$p < 0.05$, **$p < 0.01$ and ***$p < 0.001$).

5.2 Experimental procedures for the study of connection between pyramidal cells and fluorescent SOM+ interneurons.

5.2.1 Animals

The study of connection between PYR cells and SOM+ GFP+ interneurons was performed using the transgenic strain FVB-Tg(GadGFP)45704Swn/J. Transgenic mice were originally created by Oliva et al (2000) injecting a transgenic construct containing a 5' portion of the mouse *Gad1* gene, a GFP open reading frame, and SV40 polyadenylation site sequence into fertilized FVB/N mouse eggs. Mice homozygous for the TgN(GadGFP)45704Swn transgene express enhanced green fluorescent protein

(EGFP) under the control of the mouse Gad1 (GAD67) gene promoter. Homozygous mice exhibit no apparent physical or behavioral defects. Transgene expression occurs in a specific subpopulation of hippocampal and cortical GABAergic interneurons that express somatostatin.

5.2.2 Thalamocortical slices preparation

Solutions and preparation of thalamocortical slices were the same of those explained above for coronal slices preparations. The only exceptions are represented by the absence of minocycline in the sACSF solution and the cut of the brain. After its removal from the scull the brain (anterior to the tectum) was laid on a 10 º ramp. The tissue was placed with the ventral face toward the glass slide and the anterior end downhill. The ramp was placed on a protractor and a hand-held single edge razor blade was used to make a vertical cut through the tissue at an angle of 55º to the right of the posterior-to-anterior axis of the brain. The plane of cut was in this way determined by two angles: the ramp tilt angle of 10º and the blade rotation angle of 55º. The tissue rostra1 to the cut was discarded and the remaining tissue was glued onto the stage of the vibroslicer with the cut surface down and the pial surface toward the blade.
The exposed brain surface was frequently irrigated with ice-cold with sACSF during the whole dissecting procedure (Agmon and Connors; 1991). 350 µm-thick slices were then cut in the vibratome slices.

5.2.3 Patch clamp set up and recordings

The study of connection between layer 2/3 PYR cells and fluorescent somatostatin-positive interneurons were performed on somatosensory cortex from 350 µm thalamocortical slices. Neurons were recorded at 45-60 µm depth.
During the experiments, the slices were put in a chamber and continuously perfused with fresh extracellular sACSF at room temperature saturated with 95% O_2 and 5% CO_2 at 3 ml/min.
Electrical signals were recorded through a Multiclamp 700B patch-clamp amplifier and digitized using a Digidata 1322A interface and pClamp software (all from Axon Instruments). Signals were sampled at 10 kHz and filtered at 4 kHz and. Experiments were performed at room temperature.

The pipettes for patch-clamp were obtained from borosilicate capillaries (Wiretrol II 5-000-2050) using the puller P-95 (Sutter Instruments). The resistance of pipettes in the bath ranged between 3 and 5 MΩ.

Layer 2/3 PYR cells of the barrel cortex were identified on the basis of the distinct morphology characterized by triangular soma, a main apical dendrite pointing towards the *pia* and the absence of a main dendrite in the opposite direction. When possible, the morphology of neurons was confirmed by post-fixation staining of the biocytin introduced through the patch electrode. The characteristic action potential (AP) firing induced by suprathreshold current injections of increasing amplitudes in current-clamp was the main parameter used during the recordings to distinguish the type of cells. The firing of pyramidal cells shows a classic spike frequency adaptation and the maximal frequency of firing is close to 20 Hz where the second AP is wider than the first one. The firing of PYR cells is often characterized by the development of an adaptive hump as the cell is further depolarized.

Layer 2/3 fluorescent SOM^+ interneurons (SOM^+) were identified on the basis of their fluorescence response. When possible, the excitability properties were studied by induction of repetitive firing with sustained (1 s) pulses of current injection of varying intensity.

Cells selected for paired recording were less than 100 µm far from each others.

Seal was formed for each cell (the deepest one first) and then membrane patches were removed by suction in both cells sequentially.

Firing properties of pre- and postsynaptic cells were studied when possible. Once a connected pair was found, connection properties were studied using whole cell double patch-clamp recordings.

The unitary inhibitory synaptic connections were studied under paired recordings by applying 5 short pulses of suprathreshold current (20 Hz) in the presynaptic SOM^+ interneuron (in current clamp) and measuring the evoked unitary inhibitory postsynaptic currents (uIPSCs) in the postsynaptic PYR cell held at 0 mV (in voltage clamp).

Internal solution of the SOM^+ interneuron: 6 KCl, 129 KGluconate, 10 Hepes, 10 NaPhosphocreatine, 4 MgATP, 0,3 NaGTP, 0,2 EGTA, biocytin (1mg/ml), pH 7,4.

Internal solution of the PYR cell in the study of inihibitory SOM^+-PYR connections: 6 KCl, 129 CsMetansulfonate, 10 Hepes, 10 NaPhosphocreatine, 4 MgATP, 0,3 NaGTP, 0,2 EGTA, biocytin (1mg/ml), pH 7,4.

The unitary excitatory synaptic connections were studied under paired recordings by applying 5 short pulses of suprathreshold current (25 Hz) in the presynaptic PYR cell

held at -70 mV (in current clamp) and measuring the evoked unitary excitatory postsynaptic potentials (uEPSPs) in the postsynaptic SOM^+ interneuron held at -70 mV (in current clamp).

Internal solution of SOM^+ interneuron was the same described above for the study of inhibitory connection.

Internal solution of the PYR neuron in the study of excitatory PYR-SOM^+ connections: 6 KCl, 129 KGluconate, 10 Hepes, 10 NaPhosphocreatine, 4 MgATP, 0,3 NaGTP, biocytin (1mg/ml), pH 7,4.

A pharmacological approach with specific Ca2+ channel blockers was used to investigate the involvement of Ca2+ channels in controlling the neurotransmitter release at both excitatory and inhibitory synapses.

P/Q-type Ca^{2+} channel contribution was determined by applying saturating concentration of specific blocker ω-agatoxin IVA (400 nM) in the extracellular solution during consecutive trials of stimulation. The same approach was used by applying saturating concentration of specific Ca^{2+} channels blocker ω-conotoxin GVIA to determine the involvemet of N-type Ca^{2+} channels in neurotransmitter release at both excitatory and inhibitory synapse. The percentage of inhibition was calculated between the mean responses elicited by the first presynaptic AP of the train before application of toxin and after 10 minutes of toxin perfusion. The number of consecutive sweeps used for the means is variable (at least 30 consecutive trials were used).

5.2.4 Data analysis

Data analysis was performed using Igor Pro 5.0. The mean peak EPSP and IPSP amplitudes and PPR for each experiment were calculated after averaging over all the sweeps recorded without run-down. The first peak amplitude was averaged over a 1 ms window (20 points) around the peak. For each consecutive response, the previous PSP was fitted with a double-exponential decay and subtracted from the trace. For quantification of the percentage of failures, each trace was visually inspected with Clampfit 9.0 software of the pClamp suite (Axon Instruments).

The CV was calculated for each experiment from the scatter of the single synaptic responses. For each sweep the peak amplitude of the EPSP was taken as the difference between the peak during the 10 ms after the onset of the response and the baseline immediately before it. The standard deviation (SD) was calculated as in Scheuss et al.

(2002). First, the differences of the amplitudes of two successive sweeps was calculated for all sweeps. The SD was then computed as the average of these differences.

$SD^2=(1/(R-1))*\Sigma_i (A_i-A_{i+1})^2/2$

with i varying from 1 to (R-1). R is the number of trials and A_i is the amplitude of the i^{th} response.

We used this type of calculation to avoid artefacts due to long term trends or drifts of the response during recordings.

Averages were calculated with Microsoft Excel, Igor Pro 5.0. Graphs and statistical comparison were obtained with the Origin software (Microcal Software, Inc.). Data are given as mean ± SEM

5.3 Morphological reconstruction of neurons

Biocytin staining was used to confirm the morphology of cortical pyramidal cells. The morphology of soma and dendritic tree of SOM^+ interneurons was also assessed.

Biocytin is a dipeptide obtained by the condensation of biotin with the amino acid L-lysine. This dipeptide is added to intracellular medium in order to allow diffusion within the recorded neurons.

The ABC reagent used for staining (PK-7200 SIGMA) contains avidin (a glycoprotein of 68 kDa which binds with high affinity biotin: 10-15 M^{-1}) and Avidin and Byotinylated Macromolecular Complex horseradish peroxidase. Each complex has at least one binding site for biotin. ABC reagent can bind through this site biocytin contained in the recorded cell.

The presence of the complex is then detected by a colorimetric reaction catalyzed by peroxidase with chromogen DAB (diaminobenzidine tetrahydrochloride, SIGMA D7554) that produces a brown insoluble precipitate.

The staining is performed on brain slices previously fixed in 2% paraformaldehyde (at 4 ° C for a period ranging from 24 hours up to 5 days). The staining starts with 4 washes in 0.15 M phosphate buffer in order to remove the paraformaldehyde, then an incubation for 15 minutes with 3% H_2O_2 in order to inactivate endogenous peroxidase, and a set of 5 washes in phosphate buffer, after which the slices are permeabilized with 2% Triton X100 in phosphate buffer for an hour. This is then followed by incubation with ABC reagent (in 1% Triton X100 for 2 hours at room temperature or overnight at

4°C). A series of washes in phosphate buffer is then performed to remove excess reagent, followed by the staining with DAB (1:20 DAB in phosphate buffer and 0.01% H_2O_2).

At the end of the staining, the slices are mounted with Mowiol mounting medium on glass slides.

Reference list

Abbott, L.F., and Regehr, W.G. (2004). Synaptic computation. Nature 431, 796-803.

Agmon, A., and Connors, B.W. (1991). Thalamocortical responses of mouse somatosensory (barrel) cortex in vitro. Neuroscience 41, 365-379.

Ali, A.B., and Nelson, C. (2006). Distinct Ca2+ channels mediate transmitter release at excitatory synapses displaying different dynamic properties in rat neocortex. Cereb. Cortex 16, 386-393.

Amzica, F., and Steriade, M. (1995). Short- and long-range neuronal synchronization of the slow (< 1 Hz) cortical oscillation. J. Neurophysiol. 73, 20-38.

Bazhenov, M., Timofeev, I., Steriade, M., and Sejnowski, T.J. (2002). Model of thalamocortical slow-wave sleep oscillations and transitions to activated States. J. Neurosci. 22, 8691-8704.

Bolay, H., Reuter, U., Dunn, A.K., Huang, Z., Boas, D.A., and Moskowitz, M.A. (2002). Intrinsic brain activity triggers trigeminal meningeal afferents in a migraine model. Nat. Med. 8, 136-142.

Canals, S., Makarova, I., Lopez-Aguado, L., Largo, C., Ibarz, J.M., and Herreras, O. (2005). Longitudinal depolarization gradients along the somatodendritic axis of CA1 pyramidal cells: a novel feature of spreading depression. J. Neurophysiol. 94, 943-951.

Catterall, W.A. (2011). Voltage-gated calcium channels. Cold Spring Harb Perspect. Biol. 3, a003947.

Catterall, W.A., Kalume, F., and Oakley, J.C. (2010). NaV1.1 channels and epilepsy. J. Physiol. 588, 1849-1859.

Catterall, W.A., and Few, A.P. (2008). Calcium channel regulation and presynaptic plasticity. Neuron 59, 882-901.

Catterall, W.A., Perez-Reyes, E., Snutch, T.P., and Striessnig, J. (2005). International Union of Pharmacology. XLVIII. Nomenclature and structure-function relationships of voltage-gated calcium channels. Pharmacol. Rev. 57, 411-425.

Chutkow, J.G. (1974). Metabolism of magnesium in central nervous system. Relationship between concentrations of magnesium in cerebrospinal fluid and brain in magnesium deficiency. Neurology 24, 780-787.

de Kock, C.P., Bruno, R.M., Spors, H., and Sakmann, B. (2007). Layer- and cell-type-specific suprathreshold stimulus representation in rat primary somatosensory cortex. J. Physiol. 581, 139-154.

Dugue, G.P., Dumoulin, A., Triller, A., and Dieudonne, S. (2005). Target-dependent use of co-released inhibitory transmitters at central synapses. J. Neurosci. 25, 6490-6498.

Ertel, E.A., Campbell, K.P., Harpold, M.M., Hofmann, F., Mori, Y., Perez-Reyes, E., Schwartz, A., Snutch, T.P., Tanabe, T., Birnbaumer, L., Tsien, R.W., and Catterall, W.A. (2000). Nomenclature of voltage-gated calcium channels. Neuron 25, 533-535.

Fanselow, E.E., Richardson, K.A., and Connors, B.W. (2008). Selective, state-dependent activation of somatostatin-expressing inhibitory interneurons in mouse neocortex. J. Neurophysiol. 100, 2640-2652.

Hadjikhani, N., Sanchez Del Rio, M., Wu, O., Schwartz, D., Bakker, D., Fischl, B., Kwong, K.K., Cutrer, F.M., Rosen, B.R., Tootell, R.B., Sorensen, A.G., and Moskowitz, M.A. (2001). Mechanisms of migraine aura revealed by functional MRI in human visual cortex. Proc. Natl. Acad. Sci. U. S. A. 98, 4687-4692.

Halabisky, B., Shen, F., Huguenard, J.R., and Prince, D.A. (2006). Electrophysiological classification of somatostatin-positive interneurons in mouse sensorimotor cortex. J. Neurophysiol. 96, 834-845.

Isaacson, J.S., and Scanziani, M. (2011). How inhibition shapes cortical activity. Neuron 72, 231-243.

Kandel, E.R., Schwartz, J.H., and Jessel, T. (2000) Principles of neural science (Fourth edition). Prentice-Hall International Inc.

Kapfer, C., Glickfeld, L.L., Atallah, B.V., and Scanziani, M. (2007). Supralinear increase of recurrent inhibition during sparse activity in the somatosensory cortex. Nat. Neurosci. 10, 743-753.

Kawaguchi, Y., and Kondo, S. (2002). Parvalbumin, somatostatin and cholecystokinin as chemical markers for specific GABAergic interneuron types in the rat frontal cortex. J. Neurocytol. 31, 277-287.

Le Bon-Jego, M., and Yuste, R. (2007). Persistently active, pacemaker-like neurons in neocortex. Front. Neurosci. 1, 123-129.

Lauritzen, M. (2001). Cortical spreading depression in migraine. Cephalalgia 21, 757-760.

Leão, A.A.P. (1944). Spreading depression of activity in the cerebral cortex. J. Neurophysiol. 7, 359-390.

Lubke, J., and Feldmeyer, D. (2007). Excitatory signal flow and connectivity in a cortical column: focus on barrel cortex. Brain Struct. Funct. 212, 3-17.

Ma, Y., Hu, H., Berrebi, A.S., Mathers, P.H., and Agmon, A. (2006). Distinct subtypes of somatostatin-containing neocortical interneurons revealed in transgenic mice. J. Neurosci. 26, 5069-5082.

Markram, H., Toledo-Rodriguez, M., Wang, Y., Gupta, A., Silberberg, G., and Wu, C. (2004). Interneurons of the neocortical inhibitory system. Nat. Rev. Neurosci. 5, 793-807.

McGarry, L.M., Packer, A.M., Fino, E., Nikolenko, V., Sippy, T., and Yuste, R. (2010). Quantitative classification of somatostatin-positive neocortical interneurons identifies three interneuron subtypes. Front. Neural Circuits 4, 12.

Moskowitz, M.A. (2007). Genes, proteases, cortical spreading depression and migraine: impact on pathophysiology and treatment. Funct. Neurol. 22, 133-136.

Oliva, A.A.,Jr, Jiang, M., Lam, T., Smith, K.L., and Swann, J.W. (2000). Novel hippocampal interneuronal subtypes identified using transgenic mice that express green fluorescent protein in GABAergic interneurons. J. Neurosci. 20, 3354-3368.

Petersen, C.C. (2007). The functional organization of the barrel cortex. Neuron 56, 339-355.

Petersen, C.C., Hahn, T.T., Mehta, M., Grinvald, A., and Sakmann, B. (2003). Interaction of sensory responses with spontaneous depolarization in layer 2/3 barrel cortex. Proc. Natl. Acad. Sci. U. S. A. 100, 13638-13643.

Petilla Interneuron Nomenclature Group, Ascoli, G.A., Alonso-Nanclares, L., Anderson, S.A., Barrionuevo, G., Benavides-Piccione, R., Burkhalter, A., Buzsaki, G., Cauli, B., Defelipe, J., *et al.* (2008). Petilla terminology: nomenclature of features of GABAergic interneurons of the cerebral cortex. Nat. Rev. Neurosci. 9, 557-568.

Pietrobon, D. (2010b). CaV2.1 channelopathies. Pflugers Arch. 460, 375-393.

Pietrobon, D. (2010a). Insights into migraine mechanisms and CaV2.1 calcium channel function from mouse models of familial hemiplegic migraine. J. Physiol. 588, 1871-1878.

Pietrobon, D. (2007). Familial hemiplegic migraine. Neurotherapeutics 4, 274-284.

Pietrobon, D. (2005a). Migraine: new molecular mechanisms. Neuroscientist 11, 373-386.

Pietrobon, D. (2005b). Function and dysfunction of synaptic calcium channels: insights from mouse models. Curr. Opin. Neurobiol. 15, 257-265.

Pietrobon, D., and Striessnig, J. (2003). Neurobiology of migraine. Nat. Rev. Neurosci. 4, 386-398.

Reid, C.A., Bekkers, J.M., and Clements, J.D. (2003). Presynaptic Ca2+ channels: a functional patchwork. Trends Neurosci. 26, 683-687.

Rozov, A., Burnashev, N., Sakmann, B., and Neher, E. (2001). Transmitter release modulation by intracellular Ca2+ buffers in facilitating and depressing nerve terminals of pyramidal cells in layer 2/3 of the rat neocortex indicates a target cell-specific difference in presynaptic calcium dynamics. J. Physiol. 531, 807-826.

Sanchez-Vives, M.V., and McCormick, D.A. (2000). Cellular and network mechanisms of rhythmic recurrent activity in neocortex. Nat. Neurosci. 3, 1027-1034.

Scheuss, V., Schneggenburger, R., and Neher, E. (2002). Separation of presynaptic and postsynaptic contributions to depression by covariance analysis of successive EPSCs at the calyx of held synapse. J. Neurosci. 22, 728-739.

Schneggenburger, R., and Neher, E. (2005). Presynaptic calcium and control of vesicle fusion. Curr. Opin. Neurobiol. 15, 266-274.

Silberberg, G. (2008). Polysynaptic subcircuits in the neocortex: spatial and temporal diversity. Curr. Opin. Neurobiol. 18, 332-337.

Silberberg, G., and Markram, H. (2007). Disynaptic inhibition between neocortical pyramidal cells mediated by Martinotti cells. Neuron 53, 735-746.

Somjen, G.G. (2001). Mechanisms of spreading depression and hypoxic spreading depression-like depolarization. Physiol. Rev. 81, 1065-1096.

Steriade, M., Nunez, A., and Amzica, F. (1993). A novel slow (< 1 Hz) oscillation of neocortical neurons in vivo: depolarizing and hyperpolarizing components. J. Neurosci. 13, 3252-3265.

Tottene, A., Conti, R., Fabbro, A., Vecchia, D., Shapovalova, M., Santello, M., van den Maagdenberg, A.M., Ferrari, M.D., and Pietrobon, D. (2009). Enhanced excitatory transmission at cortical synapses as the basis for facilitated spreading depression in Ca(v)2.1 knockin migraine mice. Neuron 61, 762-773.

Tottene, A., Fellin, T., Pagnutti, S., Luvisetto, S., Striessnig, J., Fletcher, C., and Pietrobon, D. (2002). Familial hemiplegic migraine mutations increase Ca(2+) influx through single human CaV2.1 channels and decrease maximal CaV2.1 current density in neurons. Proc. Natl. Acad. Sci. U. S. A. 99, 13284-13289.

Tottene, A., Urbani, A., and Pietrobon, D. (2011). Role of different voltage-gated Ca2+ channels in cortical spreading depression: specific requirement of P/Q-type Ca2+ channels. Channels (Austin) 5, 110-114.

Tottene, A., Volsen, S., and Pietrobon, D. (2000). alpha(1E) subunits form the pore of three cerebellar R-type calcium channels with different pharmacological and permeation properties. J. Neurosci. 20, 171-178.

Turrigiano, G.G., and Nelson, S.B. (2004). Homeostatic plasticity in the developing nervous system. Nat. Rev. Neurosci. 5, 97-107.

van den Maagdenberg, A.M., Pietrobon, D., Pizzorusso, T., Kaja, S., Broos, L.A., Cesetti, T., van de Ven, R.C., Tottene, A., van der Kaa, J., Plomp, J.J., Frants, R.R., and Ferrari, M.D. (2004). A Cacna1a knockin migraine mouse model with increased susceptibility to cortical spreading depression. Neuron 41, 701-710.

Wang, Y., Toledo-Rodriguez, M., Gupta, A., Wu, C., Silberberg, G., Luo, J., and Markram, H. (2004). Anatomical, physiological and molecular properties of Martinotti cells in the somatosensory cortex of the juvenile rat. J. Physiol. 561, 65-90.

Wu, L.G., Westenbroek, R.E., Borst, J.G., Catterall, W.A., and Sakmann, B. (1999). Calcium channel types with distinct presynaptic localization couple differentially to transmitter release in single calyx-type synapses. J. Neurosci. 19, 726-736.

Xu, X., Roby, K.D., and Callaway, E.M. (2006). Mouse cortical inhibitory neuron type that coexpresses somatostatin and calretinin. J. Comp. Neurol. 499, 144-160.

Zaitsev, A.V., Povysheva, N.V., Lewis, D.A., and Krimer, L.S. (2007). P/Q-type, but not N-type, calcium channels mediate GABA release from fast-spiking interneurons to pyramidal cells in rat prefrontal cortex. J. Neurophysiol. 97, 3567-3573.

Zhang, X., Levy, D., Noseda, R., Kainz, V., Jakubowski, M., and Burstein, R. (2010). Activation of meningeal nociceptors by cortical spreading depression: implications for migraine with aura. J. Neurosci. 30, 8807-8814.

Zhang, E.T., Hansen, A.J., Wieloch, T., and Lauritzen, M. (1990). Influence of MK-801 on brain extracellular calcium and potassium activities in severe hypoglycemia. J. Cereb. Blood Flow Metab. 10, 136-139.

Zucker, R.S., and Regehr, W.G. (2002). Short-term synaptic plasticity. Annu. Rev. Physiol. 64, 355-405.

ABBREVIATIONS

ACh: acetylcholine

AP: action potential

ATP: adenosine-5'-triphosphate

BOLD: blood oxygenation level-dependent

Ca^{2+}: calcium

CGRP: calcitonin gene-related peptide

Cl^-: chloride

CSD: cortical spreading depression

CV: coefficient of variation

DHP: dihydropyridine

DIC: differential interference contrast

EA2: episodic ataxia type 2

EGTA: ethylene glycolbis (b-aminoethyl ether) N,N,N',N'-tetraacetic acid

EPSC: excitatory postsynaptic current

EPSP: excitatory postsynaptic potential

FHM1: familial hemiplegic migraine type 1

FITC: fluorescein isothiocyanate

FS: fast-spiking

GABA: γ-amimobutyric acid

GCS: Gluconate cutting solution

GFP: green fluorescent protein

GIN: GFP-expressing interneurons

GTP: guanosine-5'-triphosphate

HEPES: N-2-hydroethylpiperazine-N'-2-ehanesulfonic acid

HVA: high voltage activated

IPSC: inhibitory postsynaptic current

IPSP: inhibitory postsynaptic potential

IR: infrared

K^+: potassium

$[K^+]_o$: extracellular potassium concentration

KI: knock-in

LJP: liquid junction potential

LVA: low voltage activated

MA: migraine with aura

MCS: mannitol cutting solution

Mg: magnesium

MRN: magnus raphae nucleus

mACSF: modified artificial cerebrospinal fluid

Na^+: sodium

NBQX: 2,3-Dioxo-6-nitro-1,2,3,4-tetrahydrobenzo[f]quinoxaline-7-sulfonamide

NKA: neurokinin A

NMDA: N-methyl-D-aspartate

NO: nitric oxide

P: postnatal day

PAG: periaqueductal gray region

PPR: paired pulse ratio

PSC: postsynaptic current

rCBF: regional cerebral blood flow

RQ/RQ KI: homozygous R192Q knock-in

sACSF: standard artificial cerebrospinal fluid

SCA6: spinocerebellar ataxia type 6

SD: standard deviation

SOM: somatostatin

SOM^+: somatostatin positive

SP: substance P

SPG: superior sphenopalatine ganglion

SSN: superior salivatory nucleus

STD: short-term depression

TNC: trigeminal nucleus caudalis

VIP: vasoactive intestinal peptide

WT: wild-type

ω-AgaIVA: ω-agatoxin IVA

ω-CgTxGVIA: ω-conotoxin GVIA